

Dominance of the Southern Ocean in Anthropogenic Carbon and Heat Uptake in CMIP5 Models

THOMAS L. FRÖLICHER

*Environmental Physics, Institute of Biogeochemistry and Pollutant Dynamics, ETH Zürich, Zürich, Switzerland,
and Program in Atmospheric and Oceanic Sciences, Princeton University, Princeton, New Jersey*

JORGE L. SARMIENTO

Program in Atmospheric and Oceanic Sciences, Princeton University, Princeton, New Jersey

DAVID J. PAYNTER, JOHN P. DUNNE, JOHN P. KRASTING, AND MICHAEL WINTON

NOAA/Geophysical Fluid Dynamics Laboratory, Princeton, New Jersey

(Manuscript received 7 February 2014, in final form 30 September 2014)

ABSTRACT

The authors assess the uptake, transport, and storage of oceanic anthropogenic carbon and heat over the period 1861–2005 in a new set of coupled carbon–climate Earth system models conducted for the fifth phase of the Coupled Model Intercomparison Project (CMIP5), with a particular focus on the Southern Ocean. Simulations show that the Southern Ocean south of 30°S, occupying 30% of global surface ocean area, accounts for $43\% \pm 3\%$ (42 ± 5 Pg C) of anthropogenic CO₂ and $75\% \pm 22\%$ ($23 \pm 9 \times 10^{22}$ J) of heat uptake by the ocean over the historical period. Northward transport out of the Southern Ocean is vigorous, reducing the storage to 33 ± 6 Pg anthropogenic carbon and $12 \pm 7 \times 10^{22}$ J heat in the region. The CMIP5 models, as a class, tend to underestimate the observation-based global anthropogenic carbon storage but simulate trends in global ocean heat storage over the last 50 years within uncertainties of observation-based estimates. CMIP5 models suggest global and Southern Ocean CO₂ uptake have been largely unaffected by recent climate variability and change. Anthropogenic carbon and heat storage show a common broad-scale pattern of change, but ocean heat storage is more structured than ocean carbon storage. The results highlight the significance of the Southern Ocean for the global climate and as the region where models differ the most in representation of anthropogenic CO₂ and, in particular, heat uptake.

1. Introduction

The Southern Ocean is the main source of much of the deep water of the world's ocean and also provides the primary return pathway for this deep water to the surface (Toggweiler and Samuels 1995; Marshall and Speer 2012). Strongly divergent wind-driven flow drives upwelling of large amounts of deep water to the ocean's surface in the open channel around the Antarctic continent. Part of this deep water is freshened and warmed at the surface and transported northward, where it sinks into the ocean interior. The remainder of the upwelling

waters flows south and is converted to very dense Antarctic Bottom Water through cooling and brine rejection. The drawing up of deep waters and the subsequent transport into the ocean interior has major consequences for the global heat, nutrient, and carbon balances. The upwelled water takes up a large amount of excess heat from the atmosphere because it is very cold (Manabe et al. 1991). The upwelled water can also take up a large amount of anthropogenic CO₂, as it has not been in contact with the atmosphere for centuries (Mikaloff Fletcher et al. 2006; Khatiwala et al. 2009). The Southern Ocean is also the source for nutrients that fertilize a majority of the biological production in the global ocean (Sarmiento et al. 2004). The upwelled water contains a large amount of nutrients that have been accumulated in the deep ocean from the decomposition of organic matter for centuries.

Corresponding author address: Dr. Thomas L. Frölicher, Environmental Physics, Institute of Biogeochemistry and Pollutant Dynamics, ETH Zürich, Universitätstrasse 16, 8092 Zürich, Switzerland.

E-mail: thomas.froelicher@usys.ethz.ch

DOI: 10.1175/JCLI-D-14-00117.1

Given this key role of the Southern Ocean in the climate system, reports of recent and projected changes have raised significant concern. Observed changes over the last few decades include the following: (i) accelerating of the Southern Ocean overturning, possibly related to a poleward intensification of the westerly winds due to increasing greenhouse gas concentrations and polar stratospheric ozone depletion (Waugh et al. 2013; Thompson et al. 2011); (ii) subsurface warming at a faster rate and to greater depth than the global average (Gille 2002); (iii) large-scale freshening of the surface ocean (Böning et al. 2008) likely caused by significant Antarctic ice mass loss (Rignot et al. 2008), sea ice melting, and surface water flux increase; and (iv) warming, freshening, and slowdown of Antarctic bottom water formation (Purkey and Johnson 2012) that may have contributed to the recent slowdown in global surface temperature warming (Meehl et al. 2011). It has been suggested that the accelerating of the Southern Ocean overturning and the associated increase in upwelling of carbon-rich deep waters have caused a stalling of the Southern Ocean CO₂ sink despite an increase in atmospheric CO₂ and despite an increase in the subduction of mode and intermediate water (e.g., Le Quéré et al. 2007; Lovenduski et al. 2008; Lenton et al. 2009). Coupled model simulations of the twenty-first century climate consistently project a trend toward poleward amplified westerly winds and warmer sea surface temperature. It is therefore possible that a further weakening of the Southern Ocean CO₂ sink may occur (Roy et al. 2011), although increased nutrient delivery to the surface and changing surface water properties would also alter the efficiency of the biological pump (Steinacher et al. 2010). The consequence of this reduced CO₂ uptake would be a higher level of atmospheric CO₂ on multicentury time scales. The Southern Ocean will also likely experience an increase in stratification and a reduction in vertical mixing that may reduce the upward flux of natural CO₂ and the downward flux of anthropogenic CO₂ (Sarmiento et al. 1998), making it difficult to project the impact of stratification on the total CO₂ sink.

Coupled carbon–climate Earth system models are currently one of the main tools we have to investigate Southern Ocean dynamics and changes in anthropogenic CO₂ and heat uptake and storage. The remoteness and hostility of the Southern Ocean environment makes the availability of observations too sparse and interpretive frameworks too uncertain to develop a full picture of Southern Ocean heat and carbon balances (Lenton et al. 2006; Majkut et al. 2014a). Earlier-generation coupled climate models, however, poorly represent important metrics of the Southern Ocean circulation, such as the strength and position of the

westerlies, circumpolar deep water and Antarctic Bottom Water formation, mixed-layer depths, and atmosphere–ocean interactions (e.g., Doney et al. 2004; Russell et al. 2006; Sen Gupta et al. 2009; Downes et al. 2010; Trenberth and Fasullo 2010a). The large disagreement between models in representing Southern Ocean physical processes may also lead to large differences in simulated anthropogenic CO₂ and heat uptake (Orr et al. 2001; Doney et al. 2004; Russell et al. 2006).

The fifth phase of the Coupled Model Intercomparison Project (CMIP5) coupled carbon–climate Earth system model simulations give us the unique opportunity to assess CO₂ and heat uptake and storage in a large numbers of comprehensive models and for the first time in a physically self-consistent coupled setting. We focus here on the anthropogenic CO₂ component—that is, that part of the net air–sea CO₂ balance that is driven directly by the emission of CO₂ by anthropogenic activities—and the excess heat component (i.e., the change in heat uptake and storage since preindustrial times). We investigate the oceanic uptake, transport, and storage of anthropogenic carbon and heat in historical simulations from 19 Intergovernmental Panel on Climate Change (IPCC)-class CMIP5 coupled climate models with our main objectives being as follow: (i) characterizing the role of the Southern Ocean, (ii) analyzing the range between the individual models, and (iii) comparing the models with observation-based estimates. We also make use of ensemble historical simulations from a single climate model to compare intramodel variability from ensemble simulations against intermodel differences. This allows us to test to what degree the differences between the models are due to internal variability in the Southern Ocean of the various models, as each model simulates its own intrinsic variability.

We focus on analyzing changes in uptake and storage of anthropogenic carbon and heat in concert. Earlier studies often treated anthropogenic carbon and heat uptake and storage as passive processes (e.g., Bryan 1969; Church et al. 1991). Under such an assumption, ocean carbon observations may be used to estimate ocean heat uptake, or vice versa. The similarity between ocean heat and carbon uptake also underpins the concept of transient climate response to cumulative carbon emissions (e.g., Matthews et al. 2009), which suggests that the transient global warming is nearly proportional to cumulative carbon emissions on multidecadal-to-millennial time scales. Recent studies, however, showed that oceanic storage of anthropogenic carbon and heat have distinct patterns, which is not consistent with the view of passive processes acting on both anthropogenic carbon and heat (Banks and Gregory 2006; Xie and Vallis 2012; Winton et al. 2013). Winton et al. (2013) held ocean circulations fixed within a coupled carbon–climate model to

TABLE 1. Models used in the analysis.

Model	Expansion
CNRM-CM5	Centre National de Recherches Météorologiques Coupled Global Climate Model, version 5
IPSL-CM5A-LR	L'Institut Pierre-Simon Laplace Coupled Model, version 5A, low resolution
IPSL-CM5A-MR	L'Institut Pierre-Simon Laplace Coupled Model, version 5A, mid resolution
IPSL-CM5B-LR	L'Institut Pierre-Simon Laplace Coupled Model, version 5B, low resolution
FGOALS-s2	Flexible Global Ocean–Atmosphere–Land System Model, second spectral version
MIROC-ESM-CHEM	Model for Interdisciplinary Research on Climate, Earth System Model, Chemistry Coupled
MIROC-ESM	Model for Interdisciplinary Research on Climate, Earth System Model
MIROC5	Model for Interdisciplinary Research on Climate, version 5
HadGEM2-CC	Hadley Centre Global Environment Model, version 2—CarbonCycle
MPI-ESM-LR	Max Planck Institute Earth System Model, low resolution
MPI-ESM-MR	Max Planck Institute Earth System Model, medium resolution
MRI-CGCM3	Meteorological Research Institute Coupled Atmosphere–Ocean General Circulation Model, version 3
GISS-E2-R	Goddard Institute for Space Studies Model E2, coupled with the Russell ocean model
CCSM4	Community Climate System Model, version 4
NorESM1-M	Norwegian Earth System Model, version 1 (intermediate resolution)
NorESM1-ME	NorESM1-M with carbon cycling (and biogeochemistry)
GFDL CM3	Geophysical Fluid Dynamics Laboratory Climate Model, version 3
GFDL-ESM2G	Geophysical Fluid Dynamics Laboratory Earth System Model with Generalized Ocean Layer Dynamics (GOLD) component
GFDL-ESM2M	Geophysical Fluid Dynamics Laboratory Earth System Model with Modular Ocean Model, version 4 component

show that changes in ocean circulation have a much larger influence on the heat storage pattern than on the carbon storage pattern, because the relative magnitude of the natural gradient to the anthropogenic change is much larger for heat than for carbon. A slowdown of the Atlantic meridional overturning circulation, for example, may reduce the northward ocean transport of heat and, thus, shifts the heat uptake from low to high latitude (Winton et al. 2013). This shift in ocean heat uptake substantially reduces global warming even without a change in the magnitude of total heat uptake (Winton et al. 2013; Frölicher et al. 2014). Here we identify further possible mechanisms with a focus on the Southern Ocean and assess the degree to which these earlier results are robust across a wide range of climate models.

The remainder of this paper is organized as follows: Section 2 presents the coupled carbon–climate Earth system models, the processing of the model data, and the observation-based estimates. The simulated uptake, transport, and storage of anthropogenic carbon and heat are examined in sections 3a and 3b. Comparison of carbon and heat uptake and storage are discussed in section 3c. The discussion and conclusions are given in section 4. More details about the drifts in the model control simulations and about model performances are presented in the appendixes.

2. Methods

a. CMIP5 models

We use output from 19 CMIP5 models (full model names and data are provided in Tables 1 and 2; Taylor et al. 2012). The selection of the 19 models was

based on the availability of all variables necessary to discuss changes in Earth's energy system. Of those selected, 12 of the CMIP5 models—herein referred to as coupled carbon–climate Earth system models—couple the climate system to a representation of both the land and the ocean carbon cycle (marked with asterisks in Table 2). These 12 models are used for the carbon analysis, whereas all 19 models are used for the heat analysis. The horizontal resolution in the ocean ranges from $0.4^\circ \times 0.4^\circ$ to $2.0^\circ \times 2.0^\circ$ and in the atmosphere from $0.9^\circ \times 1.3^\circ$ to $2.8^\circ \times 2.8^\circ$. The numbers of vertical levels varies from 24 to 80 in the atmosphere and from 30 to 63 in the ocean. The climate models differ in many aspects (e.g., subgrid-scale parameterizations, aerosol representation, and ocean biogeochemistry). Thus, any attribution of differences between the models to potential parameters or parameterizations must be taken with caution. Some models share the same parameterizations of processes, simplifications, and numerical approximations, or even the same ocean, sea ice, land, or atmospheric components, possibly leading to similar biases (Knutti et al. 2013). Thus, the uncertainty based on the multimodel spread (one standard deviation) may be biased by the similarities between the models and the distribution of CMIP5 model output for a specific variable. For example, the analysis of the sensitivity of oceanic CO_2 uptake to climate variability and change [section 3a(4)] is based on four models only, and two models (GFDL ESMs) share the same atmosphere, land, and biogeochemical components.

We analyze historical simulations of a single-ensemble realization over the period 1861–2005 [referred to as

TABLE 2. Changes in cumulative oceanic anthropogenic carbon and heat uptake and storage south of 30°S and globally between 1870 (represented by mean of period 1861–80) and 1995 (represented by mean of period 1986–2005) simulated by the CMIP5 models. Values in brackets in the fourth row indicate global anthropogenic carbon storage for the same regions as GLODAP (Sabine et al. 2004). In the first row, asterisks (*) indicate coupled carbon–climate Earth system models, and crosses (†) indicate models for which additional simulations were available to investigate carbon–climate feedbacks.

Model	CO ₂ uptake south of 30°S (Pg C)	Carbon storage south of 30°S (Pg C)	Global carbon storage (Pg C) (GLODAP area only)	Heat uptake south of 30°S (10 ²² J)	Heat storage south of 30°S (10 ²² J)	Global heat storage (10 ²² J)	References
CNRM-CM5*	32	25	87 (79)	16			Voldoire et al. (2013)
IPSL-CM5A-LR**†	46	31	98 (91)	33	12	40	Dufresne et al. (2013)
IPSL-CM5A-MR*	52	46	112 (104)	40	25	59	Dufresne et al. (2013)
IPSL-CM5B-LR*	41	34	93 (88)	25	7	26	Dufresne et al. (2013)
FGOALS-s2				36	28	57	Bao et al. (2013)
MIROC-ESM-CHEM*	41	25	91 (84)	25	11	25	Watanabe et al. (2011)
MIROC-ESM**†	44	27	91 (84)	27	12	25	Watanabe et al. (2011)
MIROCS				18	12	22	Watanabe et al. (2010)
HadGEM2-CC*	38	28	90 (84)	19	4	−2	Martin et al. (2011)
MPI-ESM-LR*	47			21	9	36	Giorgetta et al. (2013)
MPI-ESM-MR*		34	98 (93)	18			Giorgetta et al. (2013)
MRI-CGCM3				14	6	18	Yukimoto et al. (2012)
GISS-E2-R				36	21	48	Shindell et al. (2013)
CCSM4				29	20	46	Gent et al. (2011)
NorESM1-M				24	15	27	Bentsen et al. (2012)
NorESM1-ME*	40	37	107 (99)	21	10	17	Bentsen et al. (2012)
GFDL-CM3				6	0	−25	Griffies et al. (2011)
GFDL-ESM2G**†	38	33	97 (91)	12	7	27	Dunne et al. (2012)
GFDL-ESM2M**†	42	37	104 (95)	11	10	32	Dunne et al. (2012)
CMIP5 mean ± 1 std dev	42 ± 5	33 ± 6	97 ± 8 (90 ± 7)	23 ± 9	12 ± 7	28 ± 20	

“historical” in the CMIP5 protocol (Taylor et al. 2012)] and corresponding preindustrial control simulations (piControl). The historical simulations were forced by prescribed atmospheric CO₂, non-CO₂ greenhouse gases and aerosols, stratospheric ozone depletion, and anthropogenic land-use evolution, as well as by natural forcings, such as solar and volcanic forcings. The CMIP5 models include different ozone forcing fields ranging from prescribed to prognostic stratospheric ozone changes, resulting in different response of the Southern Hemisphere westerlies to changes in stratospheric ozone. By construction, changes in land and ocean carbon storage do not feedback on atmospheric CO₂ concentration and climate, but climate and atmospheric CO₂ concentration affect land and ocean carbon storage. This is an important advance in comprehensiveness over earlier studies, in which atmospheric CO₂ is calculated explicitly from the prescribed anthropogenic carbon emissions and after the exchange with the land and ocean carbon stocks (e.g., Friedlingstein et al. 2006; Roy et al. 2011). The setup guarantees that the different ocean models “see” the same observed atmospheric CO₂ concentration.

To investigate the sensitivity of the oceanic CO₂ uptake to recent climate change, we also use simulations where atmospheric radiation experiences constant preindustrial forcing (i.e., no warming) while the ocean carbon component experiences the same increasing atmospheric CO₂ as the historical experiments [referred to as “esmFixClim2” in the CMIP5 protocol (Taylor et al. 2012); models marked with crosses in Table 2]. Differences between these simulations and the historical simulations indicate the impact of climate variability and change on CO₂ uptake. In addition, we use a six-member ensemble simulation conducted with the GFDL-ESM2G model to investigate internal variability (Dunne et al. 2012, 2013). Each of the six ensemble integrations branch off at 100-yr intervals from a stable preindustrial control simulation (Fig. A1), thus guaranteeing that they have different initial conditions. We cannot rule out, however, the possibility of a bigger uncertainty range when using a larger number of ensembles and a different magnitude of internal variability when using other models.

We regridded all model output to a regular 1° × 1° latitude–longitude grid and from sigma-depth levels to *z*-depth levels in the ocean. Although models have been spun up for several hundreds to thousands of years, the energy imbalance at the top of the atmosphere (TOA) and drifts in ocean heat and carbon storage remain significant (see appendix A for more details). Therefore, results are shown as differences between the historical simulations and the preindustrial control simulations.

We computed oceanic anthropogenic carbon by differencing dissolved inorganic carbon (DIC) of the transient historical simulation and the control simulation. Thus, the anthropogenic carbon also includes changes in the natural carbon cycle affected by anthropogenic climate perturbations, in contrast to some observation-based estimates, which by definition do not include changes in the natural carbon cycle [see section 3a(2)]. Offline global ocean biogeochemical models forced by atmospheric fields from reanalysis products suggest that changes in the natural carbon cycle over the historical period are about ± 5 Pg C (Le Quéré et al. 2010; Majkut et al. 2014a), with the Southern Ocean south of 30°S accounting for about 30% of the total change.

The global ocean heat storage changes are calculated from annual mean potential temperature of each grid cell. Temperature is converted to ocean heat storage by integrating over each model level and multiplying by a fixed value for density and heat capacity of $4.15 \times 10^6 \text{ kg m}^{-3} \text{ J K}^{-1}$.

b. Observation-based estimates of anthropogenic CO₂ and heat

We use anthropogenic carbon storage estimates that are based on the (i) ΔC* method (Gruber et al. 1996; Sabine et al. 2004), (ii) transient time distribution (TTD) method (Vaugh et al. 2006), and (iii) Green’s function approach (Khatiwala et al. 2009). The ΔC* method attempts to separate the small anthropogenic perturbation from the large background carbon storage by correcting the measured total DIC distribution for changes due to biological activities and by removing an estimate of preindustrial preformed DIC concentration. The preindustrial preformed DIC concentration is calculated on the basis of the well-known carbonate chemistry and an air–sea disequilibrium part. Unlike the ΔC* method, the TTD method and the Green’s function approach do not use DIC measurements. These methods assume that anthropogenic carbon at any point in the ocean interior should be related to the concentration history of anthropogenic CO₂ at the surface and the time it took the water parcel to reach the interior ocean location. Observed transient tracer concentrations are used to constrain the TTD or Green’s functions. There are substantial differences among the anthropogenic CO₂ estimates, especially in the Southern Ocean (Lo Monaco et al. 2005; Vázquez-Rodríguez et al. 2009; Pardo et al. 2014). For example, the TTD anthropogenic CO₂ storage in the Southern Ocean is biased high because of the assumption of constant air–sea CO₂ disequilibrium (Vaugh et al. 2006).

We also use the weighted mean anthropogenic air–sea CO₂ flux estimates of an inversion that combines

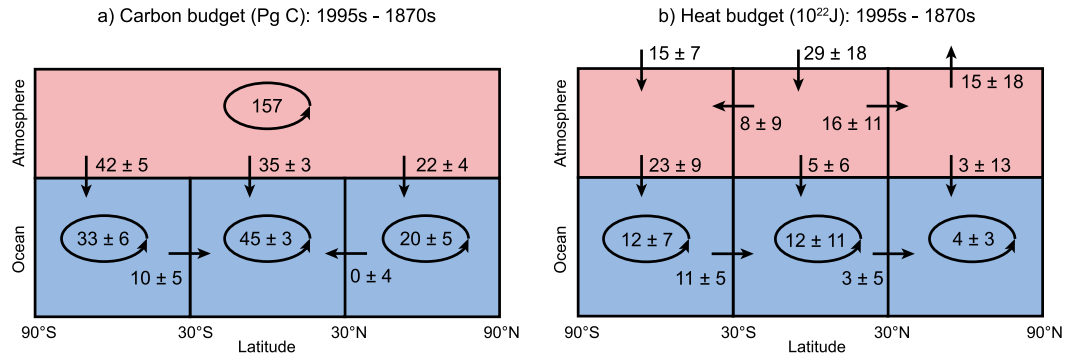


FIG. 1. Summary of CMIP5 multimodel mean changes in (a) anthropogenic carbon and (b) excess heat between 1870 (represented by mean of period 1861–80) and 1995 (represented by mean of period 1986–2005). Uncertainties represent one standard deviation between the models. The atmospheric transport of heat is the divergence of top-of-atmosphere fluxes and surface ocean fluxes, and the ocean transport of heat and carbon is the divergence of surface ocean fluxes and ocean storage. The accumulation of 157 Pg C in the atmosphere, which corresponds to an atmospheric CO₂ increase from 286 ppm in year 1861 to 379 ppm in year 2005, is prescribed in all models. Note that the heat and carbon fluxes into the ocean are not equal to their respective storage terms (imbalance of -2 ± 4 for heat and 2 ± 4 for carbon) because of nonmass conserving regridding and neglecting of small terms, such as changes in dissolved organic carbon and changes in heat storage due to friction.

data-based ΔC^* ocean interior anthropogenic carbon estimates with information about ocean transport and mixing from 10 ocean general circulation models (Mikaloff Fletcher et al. 2006). Weights represent the model skills in simulating chlorofluorocarbons successfully.

Ocean heat storage data are taken from Palmer et al. (2007), Domingues et al. (2008), Ishii and Kimoto (2009), and Levitus et al. (2009). Prior to the implementation of the Argo float network in year 2003, the ocean temperature estimates are mainly based on ship-based in situ expendable bathythermograph (XBT) measurements. The uncertainty due to the choice of XBT bias correction dominates the variability among the different methods (Lyman et al. 2010).

3. Results

We first analyze the storage, uptake, and transport of anthropogenic carbon and excess heat separately and compare the CMIP5 results with observation-based estimates. We discuss the storage first, as it is best constrained by observations. Throughout sections 3a and 3b, we discuss the CMIP5 results in the context of Fig. 1, which summarizes the simulated changes in storage, uptake, and transport of anthropogenic carbon and excess heat over the historical period.

a. Anthropogenic carbon

1) OCEANIC STORAGE OF ANTHROPOGENIC CARBON

The CMIP5 models simulate anthropogenic carbon storage of 97 ± 8 Pg C over the historical period from

1870 (represented by mean of period 1861–80) to 1995 (mean of period 1986–2005) (Table 2; Fig. 1). Storage of anthropogenic carbon is largest in the subtropical gyres, particularly in the Southern Hemisphere (Figs. 1, 2a,b). The Southern Ocean south of 30°S stores 33 ± 6 Pg C. The ocean stores less anthropogenic carbon in the tropics and the least in the high latitudes. The low storage in these regions results from the large transport of anthropogenic carbon out of these regions. The top 700 m, which account for 20% of the total global ocean volume, store 74% [or 64 ± 3 Pg C; Global Ocean Data Analysis Project (GLODAP) area only, which excludes coastal regions and several marginal seas, most notably the Arctic, the Caribbean, and the Mediterranean Sea] of the total anthropogenic carbon (Fig. 3a). A substantial amount of anthropogenic carbon is also stored below 2000 m (6% or 5 ± 3 Pg C; GLODAP area only). The well-ventilated deep waters in the Southern Ocean account for 35% of the total anthropogenic carbon below 2000 m.

The global simulated anthropogenic carbon storage of 90 ± 7 Pg C (GLODAP area only) is 15% lower than the observation-based estimate of 106 ± 17 Pg C based on the ΔC^* method (black thick line in Figs. 2a,b; Sabine et al. 2004) and is also lower than the 94–121 Pg C based on the TTD estimates (red star in Fig. 2b; Waugh et al. 2006) and the 114 ± 22 Pg C based on a Green's function approach (green square in Fig. 2b; Khatiwala et al. 2009). Models underestimate the observation-based anthropogenic carbon storage in the top 700 m, mainly in the tropics and subtropics (Figs. 2a,b, 3a). The underestimation in the subtropics of the Southern Hemisphere originates from the Southern Ocean, where

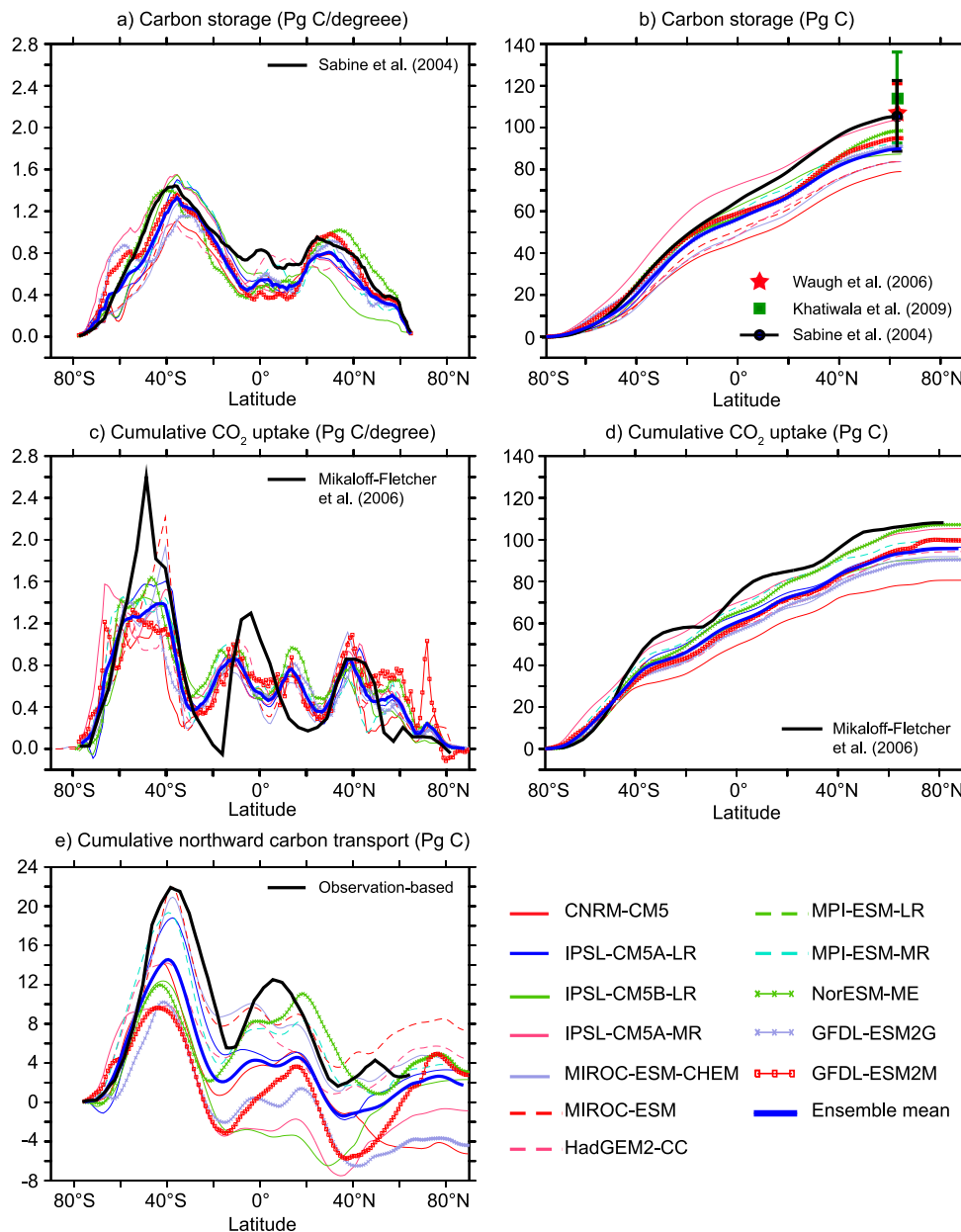


FIG. 2. Changes in oceanic storage, uptake, and transport of anthropogenic carbon between 1870 (represented by mean of period 1861–80) and 1995 (represented by mean of period 1986–2005) simulated by 12 CMIP5 models. (a) Zonal integrated oceanic anthropogenic carbon storage, (b) zonal integrated oceanic anthropogenic carbon storage integrated from 90°S to 90°N such that the vertical scale goes from 0 at 90°S to the total storage at 90°N , (c) zonal integrated cumulative ocean anthropogenic CO_2 uptake, (d) zonal integrated cumulative ocean anthropogenic CO_2 uptake integrated from 90°S to 90°N such that the vertical scale goes from 0 at 90°S to the total uptake at 90°N , and (e) northward oceanic anthropogenic carbon transport. The transport of anthropogenic carbon is the divergence of the anthropogenic CO_2 uptake and the anthropogenic carbon storage. The observation-based estimate of oceanic anthropogenic carbon transport is the divergence of the anthropogenic carbon flux estimates of Mikaloff Fletcher et al. (2006) and the anthropogenic carbon storage estimates of Sabine et al. (2004). Anthropogenic carbon storage in (a) and (b) is given for the GLODAP dataset area only, which does not cover coastal regions and several marginal seas, most notably the Arctic, the Caribbean, and the Mediterranean Sea. Excluded regions from the GLODAP area account for 7% and 10% of the total anthropogenic carbon storage in the CMIP5 models and the observation-based estimates, respectively (Table 2). Note that this has no impact when comparing results for the Southern Ocean (south of 30°S). Observation-based estimates are normalized to year 1994. Weighted mean estimates of inversion-based anthropogenic air–sea CO_2 fluxes are shown in (c) and (d).

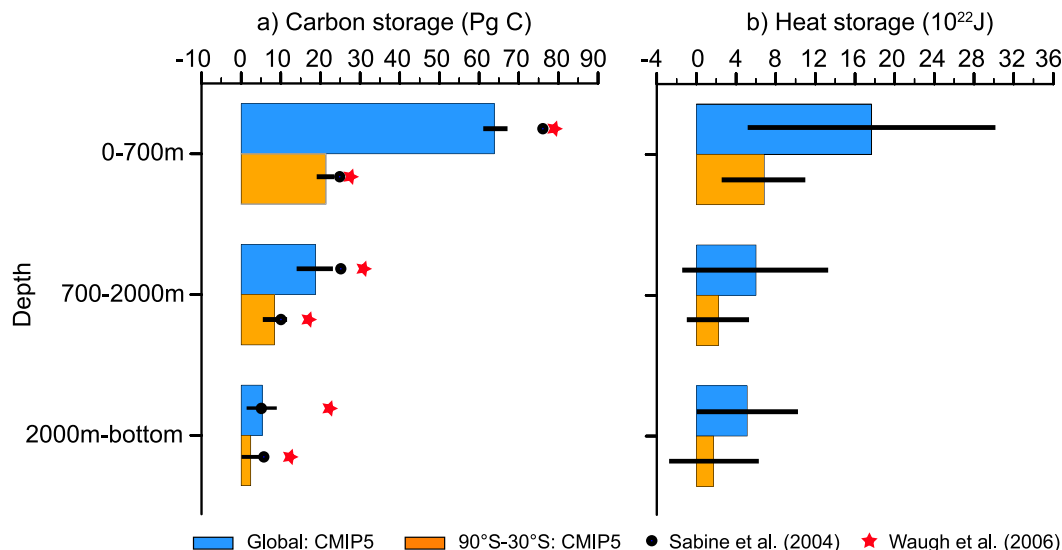


FIG. 3. CMIP5 multimodel mean changes in oceanic (a) anthropogenic carbon and (b) heat storage between 1870 (represented by mean of period 1861–80) and 1995 (represented by mean of period 1986–2005) integrated over different depth levels (0–700 m, 700–2000 m, and 2000 m–bottom) and regions (global and Southern Ocean south of 30°S). Vertical black lines indicate one standard deviation among the CMIP5 models. Observed estimates of anthropogenic carbon are based on the ΔC^* method (Sabine et al. 2004) and the TTD method (Waugh et al. 2006) and are normalized to year 1994. Note that the anthropogenic carbon estimates based on the TTD method are biased high, especially in the Southern Ocean, because of the assumption of constant air–sea CO₂ disequilibrium in this method (Waugh et al. 2006).

uptake of anthropogenic CO₂ is underestimated [see section 3a(2)]. Excluded regions in the GLODAP product account for 7 PgC (7% of the total simulated anthropogenic CO₂) in the CMIP5 models and for 12 PgC (10%) in the observation-based estimates of Sabine et al. (2004). The models and the observation-based estimates neglect the potential for increased ocean carbon storage due to carbon uptake of the land being transported into the ocean by river runoff. Regnier et al. (2013) showed that this lateral transport might have caused additional ocean storage of 10 PgC over the period 1800–2010. The impact of ocean circulation changes on anthropogenic carbon uptake, which is usually neglected in observation-based estimates, is discussed in section 3a(4).

2) OCEANIC UPTAKE OF ANTHROPOGENIC CO₂

The Southern Ocean south of 30°S accounts for 43% ± 3% (42 ± 5 PgC) of the global anthropogenic CO₂ uptake from the atmosphere from 1870 to 1995, while covering only 30% of the global ocean surface area (Figs. 1, 2c). In the Southern Ocean, the strongly divergent wind-driven flow drives upwelling of deep water with very low anthropogenic CO₂ to the surface. This water has the potential to take up a vast amount of anthropogenic CO₂ when it is exposed to the elevated atmospheric CO₂ in the presence of high wind speeds, which accelerate the uptake. The CMIP5 models also

simulate disproportionately large uptake relative to areal coverage in the southern and northern flank of the eastern equatorial Pacific upwelling region, the North Atlantic and the Kuroshio Extension (Figs. 2c,d). In contrast to the Southern Ocean, anthropogenic CO₂ uptake at midlatitudes is simulated to be low (Figs. 2c,d). The transfer of anthropogenic carbon into the ocean interior is low at these latitudes.

The broad spatial patterns of anthropogenic CO₂ uptake are consistent across the CMIP5 models, and the intermodel spread in anthropogenic CO₂ uptake is relatively small. The relatively small intermodel spread may be explained by the fact that the models are forced with the same prescribed atmospheric CO₂ boundary conditions and that the climatological large-scale ocean circulation, such as the wind-driven overturning cell in the Southern Ocean, ultimately determines the uptake of anthropogenic CO₂ over the historical period, as simulated changes in climate, ocean circulation, and thus climate–carbon feedbacks are small over the historical period. In addition, most models share similar basic chemistry equations based on the Ocean Carbon-Cycle Model Intercomparison Project Phase 2 (OCMIP-2) protocol (Watson and Orr 2003).

Most of the intermodel spread that exists stems from the Southern Ocean (Fig. 2c), most notably from 45° to 30°S, where mode and intermediate water formation

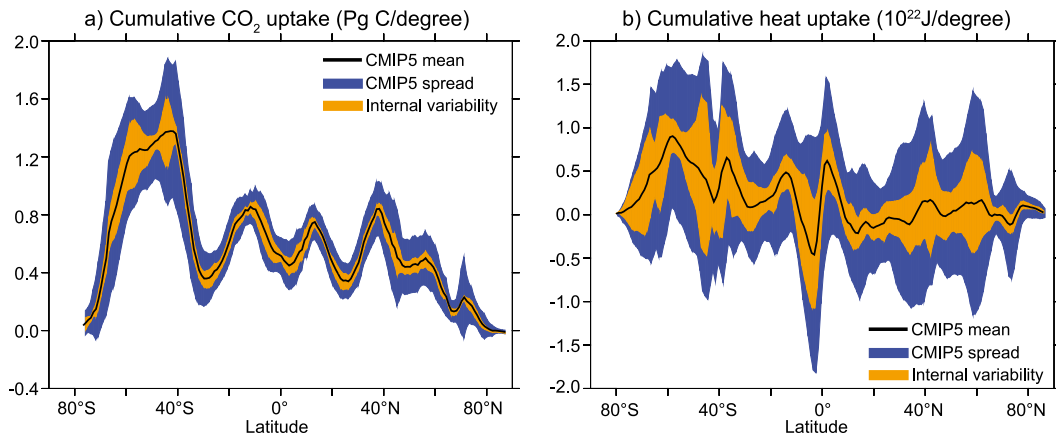


FIG. 4. The total uncertainty in CMIP5 zonal integrated changes in cumulative oceanic (a) anthropogenic CO₂ uptake and (b) excess heat uptake between 1870 (represented by mean of period 1861–80) and 1995 (represented by mean of period 1986–2005), separated into its two components: internal variability (orange; stemming from the chaotic nature of the system) and model uncertainty (blue). The total uncertainty area was calculated from adding and subtracting each uncertainty source [internal variability (orange) and model uncertainty (blue)] to and from the multimodel mean changes of the CMIP5 models. The model uncertainties are estimated as one standard deviation between the CMIP5 models, and the internal variability is estimated as one standard deviation between the six-member ensemble simulations of the GFDL-ESM2G. The ensemble simulations of GFDL-ESM2G are started with slightly different initial conditions.

occurs. For example, the CNRM-CM5 simulates the lowest cumulative anthropogenic CO₂ uptake at 30°S of 32 Pg C, whereas IPSL-CM5A-MR simulates an uptake of 52 Pg C (second column in Table 2). The maximum in the zonally integrated CO₂ uptake over the Southern Ocean differs by 25° in latitude (65°–40°S) among models. In comparison with earlier-generation OCMIP-2 and Coupled Climate Carbon Cycle Model Inter-comparison Project (C4MIP) models, however, the CMIP5 intermodel spread in anthropogenic CO₂ uptake over the Southern Ocean is significantly reduced (Watson and Orr 2003; Friedlingstein et al. 2006; Arora et al. 2013). For example, the OCMIP-2 models simulate maximum anthropogenic carbon uptake ranging from about 1.5 to 4.0 Pg C degree⁻¹ between 65° and 40°S [Fig. 5.7a in Watson and Orr (2003)], which is much larger than the CMIP5 range of about 1–2 Pg C degree⁻¹ over the same latitudinal band (Fig. 2c).

Internal variability, especially in the Southern Ocean, has to be taken into account when analyzing differences between models (Fig. 4a). Internal variability represents one standard deviation among the six ensemble members. The multimodel spread is calculated as one standard deviation among the CMIP5 models. In the Southern Ocean, internal variability accounts for 48% (averaged from 30° to 90°S) of the CMIP5 multimodel spread. Internal variability and multimodel uncertainty are generally smaller at low latitudes and in the northern high latitudes, but internal still accounts for 41% (averaged from 30°S to 90°N) of the multimodel spread.

The overall pattern of anthropogenic CO₂ uptake is in good agreement with estimates from ocean inversions based on anthropogenic oceanic CO₂ reconstructions (Fig. 2c; Mikaloff Fletcher et al. 2006). The inverse estimates show larger uptake in the Southern Ocean between 40° and 60°S, and the equatorial regions between 10°S and 10°N but smaller uptake in the subtropical gyres. On a global scale, higher ocean inversion carbon uptake can be explained by the fact that the inversion results are based on the ΔC* anthropogenic carbon storage estimates, which are larger than the simulated CMIP5 anthropogenic carbon storage [see section 3a(1)]. On a regional scale, differences may also reflect different transport pathways in the underlying ocean models used in Mikaloff Fletcher et al. (2006). The inverse studies use earlier-generation coarse-resolution ocean models with known errors in the representation of the Southern Ocean circulation. The errors have been attributed to imprecise formulation of subgrid-scale processes, the representation of transport along isopycnals, and brine rejection due to sea ice formation (Mikaloff Fletcher et al. 2006).

The CMIP5 models simulate an anthropogenic CO₂ uptake of 1.9 ± 0.2 Pg C yr⁻¹ averaged over the period 1986–2005 (Table 3). This is consistent with the anthropogenic CO₂ flux estimate of 1.9 ± 0.6 Pg C yr⁻¹ based on atmospheric O₂/N₂ measurements (Manning and Keeling 2006) and the anthropogenic CO₂ flux estimates of 2.0 ± 0.6 Pg C yr⁻¹, 2.0 ± 0.6 Pg C yr⁻¹, and 2.3 ± 0.5 Pg C yr⁻¹ based on three different methods using surface water pCO₂ measurements (Takahashi et al. 2009; Majkut et al. 2014b; Landschützer et al.

TABLE 3. Summary of global anthropogenic CO₂ uptake estimates for the period of the 1990s. The uncertainty for the CMIP5 ensemble mean estimate is given as one standard deviation between the models. Note that the ocean inversion assumes that the ocean circulation and biology are in steady state. The third row indicates an estimate of anthropogenic CO₂ uptake simulated by the four models that additionally provide a simulation with no changes in radiative forcing, but the increasing CO₂ impacts ocean CO₂ uptake [see section 3a(4) for more details]. The same four models simulate anthropogenic CO₂ uptake of 2.0 ± 0.1 Pg C yr⁻¹ when changes in radiative forcing are included.

Method	CO ₂ uptake (Pg C yr ⁻¹)	Time period	Reference
CMIP5	1.9 ± 0.2	1986–2005	This study (11 Models)
CMIP5 (CO ₂ only; no changes in radiative forcing)	2.1 ± 0.1	1986–2005	This study (4 Models)
Ocean inversion	2.2 ± 0.3	Nominal 1995	Mikaloff Fletcher et al. (2006)
O ₂ /N ₂	1.9 ± 0.6	1990–99	Manning and Keeling (2006)
Air–sea pCO ₂ difference	2.0 ± 0.6	Nominal 2000	Takahashi et al. (2009)
	2.0 ± 0.6	1998–2011	Landschützer et al. (2014)
	2.3 ± 0.5	Nominal 2000	Majkut et al. (2014b)
	2.4 ± 0.5	1990–99	Watson and Orr (2003)
OCMIP-2	2.4 ± 0.5	1990–99	Watson and Orr (2003)
OGCM (hindcast)	1.9 ± 0.3	1990–99	Wanninkhof et al. (2013)

2014). The CMIP5 estimate is also in good agreement with the 2.4 ± 0.5 Pg C yr⁻¹ estimate based on 13 OCMIP-2 forward ocean models (Watson and Orr 2003), the 1.9 ± 0.3 Pg C yr⁻¹ estimate based on recent hindcast simulations from eight ocean general circulation models (OGCM; Wanninkhof et al. 2013), and the ocean inversion estimate of 2.2 ± 0.3 Pg C yr⁻¹ based on a suite of 10 ocean general circulation models (Mikaloff Fletcher et al. 2006). The CMIP5 models as a class tend to underestimate the outgassing in the eastern equatorial Pacific and tend to slightly overestimate the uptake close to the Antarctic Continent (see appendix B for discussion and Fig. B1). Data uncertainty, however, is particularly large in the southern high latitudes (Majkut et al. 2014a).

3) OCEANIC TRANSPORT OF ANTHROPOGENIC CARBON

The transport of anthropogenic carbon is calculated as the divergence of the anthropogenic CO₂ uptake and the anthropogenic carbon storage. Overall, there is a net northward transport of anthropogenic CO₂ throughout the Southern Ocean, peaking at about 40°S from 1870 to 1995. The northward anthropogenic carbon transport at 30°S is 10 ± 5 Pg C (Figs. 1a, 2e). We find that 23% ± 10% of the 42 ± 5 Pg anthropogenic carbon that enters the Southern Ocean south of 30°S is transported northward out of the Southern Ocean, resulting in a Southern Ocean anthropogenic CO₂ storage of 33 ± 6 Pg C (Fig. 1a). The northward anthropogenic CO₂ transport continues across the equator into the Northern Hemisphere. The CMIP5 models show a northward transport of 4.3 ± 4.6 Pg C across the equator, which is primarily driven by the upper Atlantic Ocean. In the Northern Hemisphere, the southward transport at midlatitudes and the northward transport from the equator lead to

large storage in the subtropics. The variability between the models, however, is large in the subtropics of the Northern Hemisphere (Fig. 2e). In the Northern Hemisphere, the models also differ in the direction of the meridional transport.

The latitudinal distribution of the predominately northward anthropogenic carbon transport simulated by the CMIP5 models is in good agreement with the observation-based estimate (Fig. 2e) with large transport in the Southern Ocean and the North Atlantic. The simulated transport of anthropogenic carbon at 30°S of 10 ± 5 Pg C, however, is smaller than the observation-based estimate of about 19 Pg C, and the southward cross-equatorial anthropogenic CO₂ transport simulated by a subset of the CMIP5 models is in contrast to the observation-based northward cross-equatorial transport estimate. The small simulated anthropogenic carbon transport at 30°S may be associated with the small simulated anthropogenic carbon uptake south of 30°S. Note that the observation-based anthropogenic CO₂ transport is calculated as the divergence of the observation-based anthropogenic CO₂ uptake (Mikaloff Fletcher et al. 2006) and the anthropogenic CO₂ storage (Sabine et al. 2004), which both have uncertainties.

4) SENSITIVITY OF OCEANIC CO₂ UPTAKE TO CLIMATE VARIABILITY AND CHANGE

The global oceanic CO₂ uptake has been largely unaffected by climate variability and change over the historical period (Fig. 5). Note that only four models provide simulations where atmospheric radiation experiences constant preindustrial forcing while the ocean carbon component experiences increasing atmospheric CO₂. The largest reduction of 5 Pg C over the period 1870–1995 is simulated by the GFDL-ESM2M and the MIROC-ESM models, which accounts for 5% in

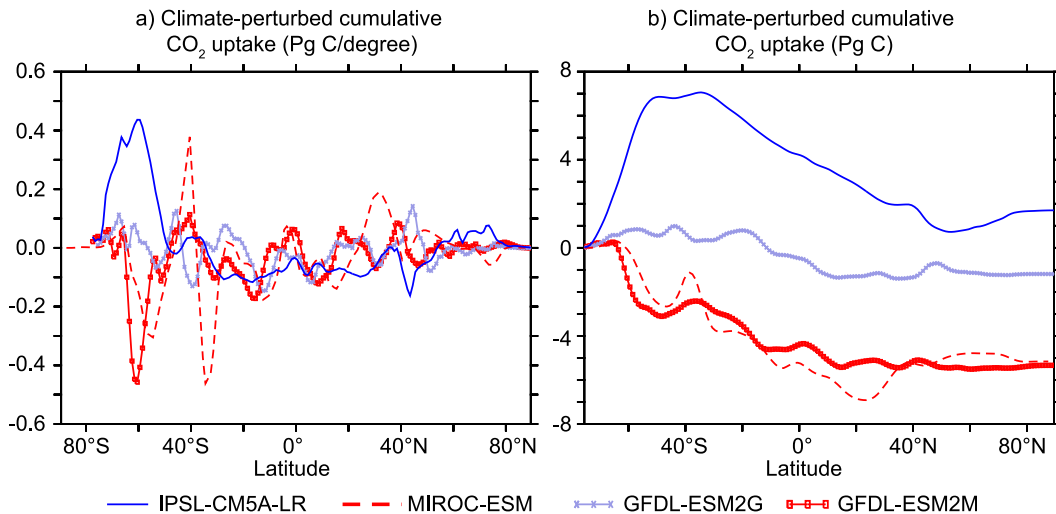


FIG. 5. Differences in cumulative oceanic CO_2 uptake between simulations with climate change and simulations without climate change but increasing CO_2 from 1870 (represented by mean of period 1861–80) to 1995 (represented by mean of period 1986–2005). (a) Zonal integrated cumulative oceanic CO_2 uptake, and (b) zonal integrated cumulative oceanic CO_2 uptake integrated from 90°S to 90°N such that the vertical scale goes from 0 at 90°S to the total uptake at 90°N . Negative values indicate a positive carbon–climate feedback (i.e., a reduced ocean carbon uptake in response to climate change and variability).

GFDL-ESM2M and 6% in MIROC-ESM of the total anthropogenic CO_2 uptake over the same period. A substantial fraction of this reduction (e.g., 54% for GFDL-ESM2M) is simulated in the Southern Ocean during the last 30 years of the simulation. Changes north of 30°N are small in all models. Climate variability and change have reduced the global anthropogenic CO_2 uptake from $2.1 \pm 0.1 \text{ Pg C yr}^{-1}$ to $2.0 \pm 0.1 \text{ Pg C yr}^{-1}$ over the period 1986–2005 (Table 3).

The IPSL-CM5A-LR shows an enhanced carbon uptake in response to climate variability and change over the historical period. The model simulates a large sudden increase in Southern Ocean carbon uptake in the 1940s in the simulation where atmospheric radiation experiences constant preindustrial forcing, possibly reflecting natural internal variability, but further investigation is needed.

The very small simulated effect of climate variability and change on the carbon uptake in the CMIP5 models on the order of 5 Pg C suggests that the underestimation of about 16 Pg C in global anthropogenic CO_2 storage in the CMIP5 models in comparison with data-based estimates using the ΔC^* method (Sabine et al. 2004) cannot be explained by the fact that the data-based estimates assume a steady-state ocean and thus do not include by design any climate-related changes in carbon uptake.

b. Excess heat

In this section, we focus on the excess heat component (i.e., the change in ocean heat storage, uptake and

transport since preindustrial times). A positive value implies a heat flux into the ocean.

1) OCEANIC STORAGE OF EXCESS HEAT

The CMIP5 models simulate global ocean heat storage change of $28 \pm 20 \times 10^{22} \text{ J}$ over the historical period from 1870 (represented by mean of period 1861–80) to 1995 (mean of period 1986–2005) (Fig. 6; Table 2). Regionally, changes in ocean heat storage are dominated by the Southern Ocean with a maximum at around 45°S and the low latitudes of the Northern Hemisphere with a maximum at around 15°N (Fig. 6b). The Southern Ocean south of 30°S stores $12 \pm 7 \times 10^{22} \text{ J}$. Changes in ocean heat storage north of 30°N are small ($4 \pm 3 \times 10^{22} \text{ J}$). Of the global ocean heat storage, 61% ($17 \pm 13 \times 10^{22} \text{ J}$) is stored in the top 700 m in the CMIP5 models, and 18% ($5 \pm 5 \times 10^{22} \text{ J}$) below 2000 m (Fig. 3b). Of this 18%, 31% ($2 \pm 4 \times 10^{22} \text{ J}$) is stored in the Southern Ocean below 2000 m. Thus, the deep Southern Ocean below 2000 m has warmed on average by about $0.03^\circ \pm 0.03^\circ\text{C}$ and accounts for about 6% of the total ocean heat storage changes over the historical period.

In contrast to simulated changes in global anthropogenic carbon storage, intermodel differences in simulated global ocean heat storage changes are very large [$\pm 8\%$ for carbon vs $\pm 71\%$ for heat (Figs. 6a,b; Table 3)]. The models also differ on sign of ocean heat storage changes. The HadGEM-CC ($-2 \times 10^{22} \text{ J}$) and the GFDL CM3 ($-25 \times 10^{22} \text{ J}$), for example, suggest a cooling over the historical period, inconsistent with

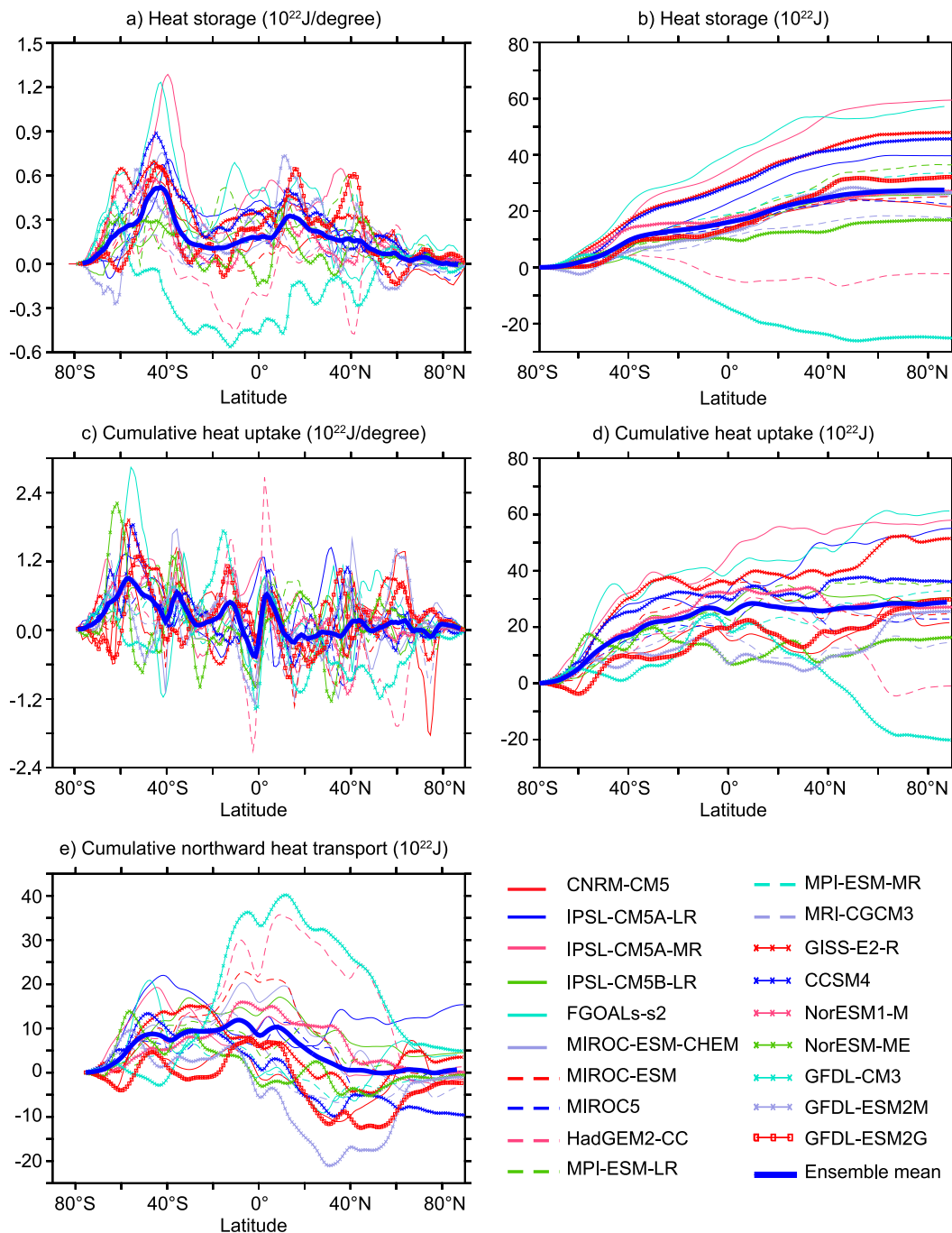


FIG. 6. Changes in oceanic storage, uptake, and transport of excess heat between 1870 (represented by mean of period 1861–80) and 1995 (represented by mean of period 1986–2005) simulated by 19 CMIP5 models. (a) Zonal integrated ocean heat storage change, (b) zonal integrated ocean heat storage change integrated from 90°S to 90°N such that the vertical scale goes from 0 at 90°S to the total storage at 90°N, (c) zonal integrated cumulative ocean heat uptake, (d) zonal integrated cumulative ocean heat uptake integrated from 90°S to 90°N such that the vertical scale goes from 0 at 90°S to the total uptake at 90°N, and (e) northward transport of heat. The transport of heat is the divergence of the change in oceanic heat uptake and the ocean heat storage.

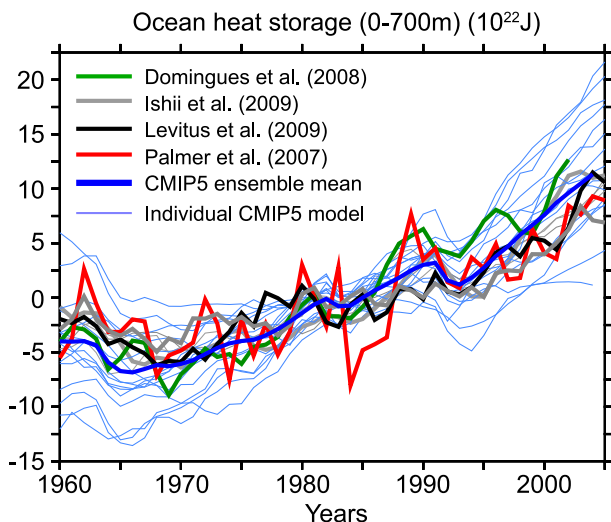


FIG. 7. Changes in annual mean global upper (top 700 m) ocean heat storage simulated by 19 CMIP5 models and based on observations. All time series are anomalies to the period 1960–2005.

recent observation-based estimates (Levitus et al. 2009). It has been shown by Zhang et al. (2013) that both models likely overestimate the strength of the aerosol indirect effects upon cloud properties, resulting in an overly negative radiative forcing over the historical period that counteracts the greenhouse gas-induced positive radiative forcing. In addition, the preindustrial control simulations from most of the CMIP5 models used in this study, including HadGEM-CC and GFDL CM3, do not include explosive volcanic eruptions. It has been shown that climate models without preindustrial volcanic forcing underestimate ocean heat uptake over the historical period (e.g., Frölicher et al. 2011; Gregory et al. 2013). The negative ocean heat storage anomaly in HadGEM-CC and GFDL CM3 might, therefore, be caused by a combination of very strong aerosol effects and the omission of episodic explosive volcanic eruptions in the preindustrial control simulation.

The individual CMIP5 models are able to reproduce the observed changes in upper-ocean heat storage from 1960 to 2005, including the variations imposed by volcanic eruptions, such as Agung in year 1963, El Chichón in year 1982, and Pinatubo in year 1991 (Fig. 7). The simulated linear trend of the CMIP5 multimodel mean of $0.37 \pm 0.22 \times 10^{22} \text{ J yr}^{-1}$ is within the range spanned by the observation-based estimates of $0.18 \times 10^{22} \text{ J yr}^{-1}$ (Levitus et al. 2009), $0.20 \times 10^{22} \text{ J yr}^{-1}$ (Ishii and Kimoto 2009), $0.25 \times 10^{22} \text{ J yr}^{-1}$ (Palmer et al. 2007), and $0.40 \times 10^{22} \text{ J yr}^{-1}$ (Domingues et al. 2008; trend over period 1960–2002).

2) OCEANIC UPTAKE OF EXCESS HEAT

The Southern Ocean plays a pivotal role for excess heat uptake: $75\% \pm 22\%$ ($23 \pm 9 \times 10^{22} \text{ J}$) of the total

ocean heat uptake over the historical period from 1870 to 1995 enters the Southern Ocean south of 30°S by a reduction in ocean to atmosphere heat flux (Figs. 1b, 6c,d). Changes in the surface heat flux are highly variable with respect to latitude (some areas even lose heat) and have a maximum over the circumpolar ocean between 45° and 65°S (Fig. 6c). South of 30°S , the excess heat uptake of $23 \pm 9 \times 10^{22} \text{ J}$ is larger than the top-of-atmosphere energy imbalance of $15 \pm 7 \times 10^{22} \text{ J}$ because of a poleward atmospheric heat transport of $8 \pm 9 \times 10^{22} \text{ J}$ in the midlatitudes of the Southern Hemisphere (Fig. 1b).

The main reason for the large uptake of excess heat by the Southern Ocean is the wind-driven upwelling of cold deep waters to the surface and the northward transport and subduction of the heated water masses into the ocean interior. The upwelling nearly anchors sea surface temperatures at preindustrial levels over the historical period between 45° and 65°S . As a result, the circumpolar ocean exhibits only small change in the longwave energy leaving the surface (Fig. 8d). This lack of sea surface temperature warming also leads to a stronger coupling between the sea surface temperature and the 2-m atmospheric temperature and a reduced loss of sensible heat from the surface (Fig. 8e). The reflected shortwave energy (Fig. 8b) also decreases over the Southern Ocean, possibly related to sea ice loss and cloud cover increase.

The variability between the models in ocean heat uptake over the historical period is large (Figs. 6c,d). For example, the GFDL-ESM2M (light blue lines with crosses in Figs. 6c,d) takes up 34% of the heat in the Southern Ocean, whereas the NorESM1-ME uptakes 117% in the Southern Ocean (green lines with crosses in Figs. 6a,b), implying a net release of excess heat by the remaining world oceans. Individual surface heat flux terms show an even larger spread among the models (Fig. 8; Table 2), suggesting a lack of consensus over how the surface energy budget has been altered since preindustrial times and which processes (e.g., cloud feedback processes and aerosol indirect effect) are driving the changes. However, the general picture associated with a warming lower atmosphere prevails (i.e., the increase in surface upward longwave radiation associated with warming SSTs and increased downward longwave radiation associated with both increased greenhouse gases and atmospheric temperature). Interestingly, the CMIP5 models as a class suggest no significant change in global precipitation over the historical period (i.e., change of $2 \pm 62 \times 10^{22} \text{ J}$ in latent heat flux, Fig. 8f) despite the increase in global mean surface temperature. A recent study uses idealized model runs in which only atmospheric CO_2 is prescribed to increase to show that CMIP5 models on average simulate an increase in latent

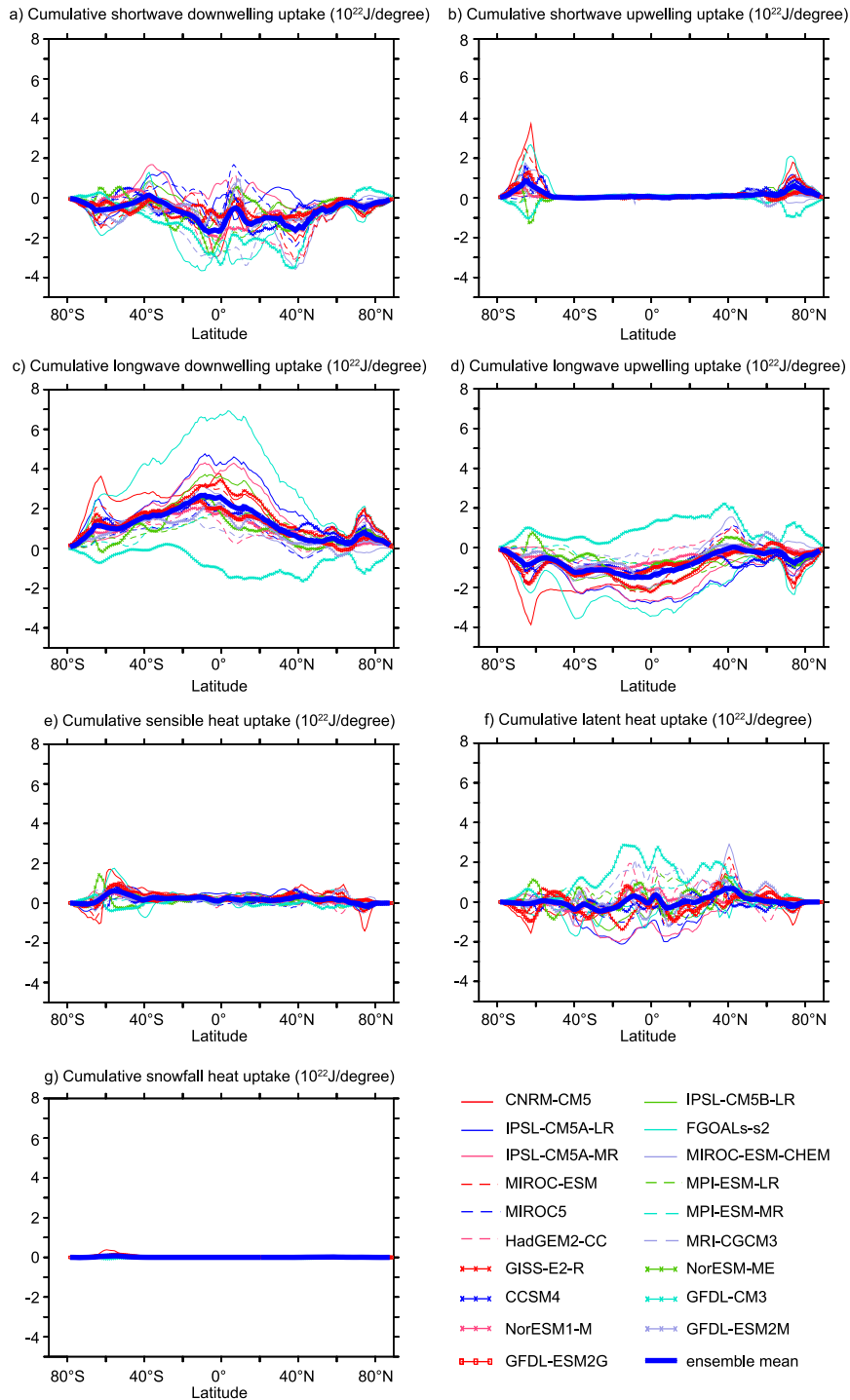


FIG. 8. Changes in cumulative (a) shortwave downwelling radiation, (b) shortwave upwelling radiation, (c) longwave downwelling radiation, (d) longwave upwelling radiation, (e) sensible heat flux, (f) latent heat flux, and (g) snowfall heat flux between 1870 (represented by mean of period 1861–80) and 1995 (represented by mean of period 1986–2005) at the surface of the ocean. Fluxes are all defined as positive into the ocean. Positive snowfall heat fluxes indicate a decrease in snowfall but were not available for all models.

heat flux as the global mean surface temperature increases (Pendergrass and Hartmann 2014). This suggests that changes in the atmospheric energy budget driven by non-CO₂ radiative forcing agents are most likely responsible for the lack of latent heat increase seen for the CMIP5 models over the 1861–2005 period.

The largest internal variability in excess heat uptake is simulated in the Southern Ocean south of 30°S (Fig. 4b). There, simulated internal variability (estimated as one standard deviation between the ensemble members) accounts for 74% (averaged from 30° to 90°S) of the CMIP5 multimodel spread (estimated as one standard deviation between the CMIP5 models) in zonal integrated cumulative heat uptake. As for anthropogenic carbon, internal variability can substantially contribute to the spread in ocean heat uptake in the CMIP5 models and has to be taken into account when analyzing differences in ocean heat uptake between multiple models and when attributing observation-based trends in ocean heat uptake to anthropogenic forcing.

3) OCEANIC TRANSPORT OF EXCESS HEAT

The CMIP5 models consistently simulate a weakening of the zonal integrated poleward heat transport at most latitudes in the Southern Hemisphere, causing a redistribution of heat from the circumpolar ocean at high southern latitudes to the low latitudes from 1870 to 1995 (Figs. 1b, 6e). $48 \pm 22\%$ of the excess heat that enters the Southern Ocean south of 30°S is transported out of 30°S into the low latitudes. The CMIP5 models simulate a northward excess heat transport across the equator of $8 \pm 10 \times 10^{22}$ J and a northward excess heat transport of $3 \pm 13 \times 10^{22}$ J at 30°N. There is substantial variability between the models in the low latitudes of the Northern Hemisphere and the Southern Ocean south of 30°S. In particular, GFDL CM3 and HadGEM2-CC have a large northward excess heat transport across the equator and north of 30°N. This is because of the highly asymmetrical radiative forcing patterns in these models resulting from very large aerosol-induced negative surface forcing in the Northern Hemisphere [see section 3b(1)].

c. Comparing oceanic uptake and storage of anthropogenic carbon and heat

Next, we analyze the spatial relationship between changes in oceanic uptake and storage of anthropogenic CO₂ and heat from 1861 to 2005 (Fig. 9).

Anthropogenic CO₂ and heat storage show a common broad-scale pattern of change (Figs. 9a–d). High levels of anthropogenic CO₂ and heat storage are simulated in the thermocline at mid–high latitudes in the Southern

Hemisphere in all ocean basins, the North Atlantic, and the subtropical North Pacific (Figs. 9a–d). Low storage of anthropogenic CO₂ and heat is simulated in the equatorial Pacific and Indian Ocean (Figs. 9a,b). The vertical distributions of anthropogenic CO₂ and heat storage show that both have their maximum in the upper few hundred meters, except in deep water formation regions, such as the Southern Ocean and North Atlantic, where anthropogenic CO₂ and heat penetrate below 700-m depth (Figs. 9c,d).

On a regional-to-local scale, the anthropogenic CO₂ storage differs largely from the excess heat storage. The ocean heat storage is overall more structured than the anthropogenic CO₂ storage (Figs. 9a–d). Large ocean heat storage is simulated between 60° and 50°S in the Indian sector of the Southern Ocean and off the coast of Argentina (Fig. 9b), where heat penetrates to greater depths (Fig. 9d). The anthropogenic CO₂ storage pattern in the Southern Ocean is much smoother than the heat storage pattern (Fig. 9a), and anthropogenic CO₂ penetrates to greater depths in a relatively wide latitudinal band between 60° and 30°S (Fig. 9c). In the low latitudes, the heat storage is restricted to the upper few hundred meters (Fig. 9d), whereas relatively high anthropogenic CO₂ storage is simulated below that. The western subtropical South Pacific at around 250-m depths and parts of the Southern Ocean, the North Atlantic, and the North Pacific even cool (Fig. 9b). In contrast, the anthropogenic CO₂ changes are generally positive (Figs. 9a,b).

The resemblance of the broad-scale anthropogenic CO₂ pattern to the excess heat pattern is less strong for uptake than for storage (Figs. 9e,f). In general, the anthropogenic CO₂ and heat uptake is large in the Southern Ocean and the North Atlantic but low in the subtropical gyres. The anthropogenic CO₂ uptake pattern appears to be much smoother than the heat uptake pattern. For example, the excess heat uptake in the Southern Ocean is very localized, in contrast to the large-scale anthropogenic CO₂ uptake. The ocean loses heat in a number of regions, which is not simulated for anthropogenic CO₂. The differences between anthropogenic CO₂ and heat can further be exemplified by comparing uptake, transport and storage in concert (Fig. 1). The northward transport of anthropogenic CO₂ out of the Southern Ocean accounts for $23\% \pm 10\%$ of the Southern Ocean anthropogenic CO₂ uptake, indicating that about three-quarters gets trapped in the Southern Ocean. In contrast, $48\% \pm 22\%$ of the Southern Ocean excess heat uptake is transported northward, and only about half of the excess heat uptake is stored in the Southern Ocean.

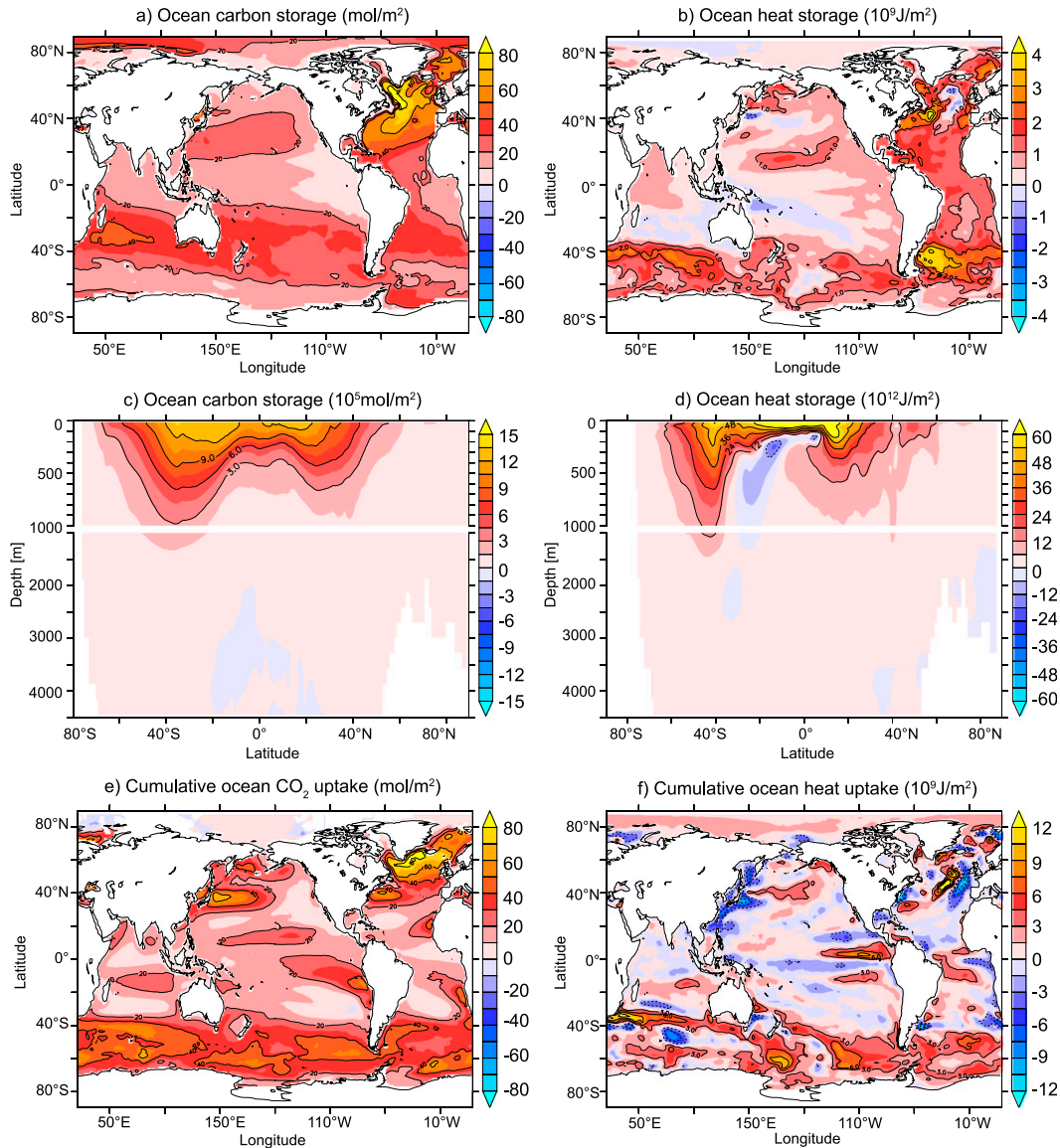


FIG. 9. CMIP5 multimodel mean changes in depth-integrated oceanic (a) anthropogenic carbon and (b) heat storage, zonal integrated (c) anthropogenic carbon and (d) heat storage, and cumulative (e) anthropogenic carbon and (f) heat uptake between 1870 (represented by mean of period 1861–80) and 1995 (represented by mean of period 1986–2005).

4. Discussion and conclusions

We assess uptake, transport, and storage of anthropogenic carbon and heat over the period 1861–2005 as simulated by the CMIP5 models. One of the key results from this analysis is that the Southern Ocean south of 30°S dominates the modeled anthropogenic CO₂ and heat uptake. As is evident from Fig. 1, the Southern Ocean takes up 43% ± 3% of the total anthropogenic CO₂ and 75% ± 22% of the heat; it covers only 30% of the total surface area. The CMIP5 models confirm

earlier studies that suggest that the Southern Ocean plays a central role in slowing the rate of global warming through the uptake of anthropogenic CO₂ and heat (Manabe et al. 1991; Sarmiento et al. 1998; Caldeira and Duffy 2000; Orr et al. 2001). In addition, large-scale patterns, such as the high anthropogenic CO₂ and heat uptake by the Southern Ocean and also the large storage of anthropogenic CO₂ there, are robust between the models (i.e., the models agree on sign of changes).

The main reason for the Southern Ocean dominance in anthropogenic CO₂ and heat uptake is its distinct

dynamical regime. The Southern Ocean provides the primary return pathway for deep waters to the surface and returns the waters back into the ocean interior predominantly north of the upwelling branch (Toggweiler and Samuels 1995; Marshall and Speer 2012). The upwelling continually exposes this cold and mostly anthropogenic carbon-free water to the now warmer and carbon-rich atmosphere, allowing for uptake of additional heat and carbon as the waters flow northward in the surface Ekman layer.

However, the regional anthropogenic CO₂ and heat uptake and storage patterns show large differences, suggesting that different mechanisms are important. For example, the northward transport of anthropogenic CO₂ out of the Southern Ocean accounts for 23% ± 10% of the Southern Ocean anthropogenic CO₂ uptake, while a higher fraction of 48% ± 22% of the Southern Ocean excess heat uptake is transported northward (Fig. 1). Banks and Gregory (2006) and Xie and Vallis (2012) use passive tracer techniques within coupled climate model simulations to show that the redistribution of the existing heat reservoir due to changes in ocean circulation and mixing plays an important role in shaping the excess heat uptake and storage pattern. Winton et al. (2013) fixed the ocean circulation in transient warming simulations with a fully coupled carbon cycle–climate model to show that ocean circulation changes have, in contrast to heat, a modest impact on the anthropogenic CO₂ uptake and storage pattern. Specifically, Winton et al. show that a weakening of the Atlantic meridional overturning circulation diminishes poleward heat transport into the North Atlantic, providing a cooling tendency at the ocean surface and enhanced ocean heat uptake. In the Southern Ocean, a reduction of deep convection with global warming causes heat to accumulate beneath the surface (Winton et al. 2013). In addition, regions of reduced warming are simulated near the equator at several hundred meters depth when circulation changes. All features are not simulated for anthropogenic CO₂ (Winton et al. 2013).

Do the CMIP5 models simulate similar patterns, which would point to an important role of ocean circulation changes in explaining the differences between anthropogenic CO₂ and heat uptake? Yes and no. In the North Atlantic, the CMIP5 models simulate both high anthropogenic CO₂ storage (Fig. 9a) and negative ocean heat storage (Fig. 9b) consistent with the Winton et al. (2013) results. Because the changes of the Atlantic meridional overturning circulation in response to global warming and the associated redistribution of the existing heat reservoir largely differ between the CMIP5 models (Cheng et al. 2013), differences in the representations of the Atlantic meridional overturning circulation may also

partly explain the differences in ocean heat uptake and storage among the models, at least in the North Atlantic. In the Southern Ocean, the CMIP5 models simulate lobes of deep ocean heat storage in a relatively narrow band (Fig. 9d) not simulated for anthropogenic CO₂. Winton et al. (2013) show that these features appear only when ocean circulation changes redistribute the existing heat reservoir (cf. Fig. 3 in Winton et al. 2013). However, in contrast to Winton et al. (2013), no enhanced ocean warming at subsurface is simulated in the CMIP5 models. The absence of this subsurface warming signal may simply reflect the fact that the simulated changes in Southern Ocean circulation and ventilation are small over the historical period. Winton et al. (2013) analyzed changes after a doubling of CO₂, and thus changes in ocean circulation are much larger. If the redistribution of the preexisting heat content due to changes in ocean circulation is the primary driver for the excess heat uptake and storage pattern (Winton et al. 2013), biases in the base state of the models as well as differences in ocean circulation changes may explain part of the differences in regional excess heat uptake and storage patterns between the models. Differences in the uptake kinetics (CO₂ is subject to solubility and carbon chemistry), differences in the air–sea equilibration time scale (nine months for CO₂; less than a month for heat), and differences in the atmospheric boundary conditions (spatially uniform and exponentially increasing for CO₂; spatially and temporal variable radiative forcing for heat) are further possible mechanisms that may cause differences between anthropogenic CO₂ and heat uptake and storage patterns. Which processes ultimately determine the differences in uptake of anthropogenic carbon and heat remains to be investigated with idealized eddy-resolving model simulations using passive heat tracers.

Our comparison with observation-based estimates shows that the CMIP5 models as a class tend to underestimate the uptake of anthropogenic CO₂ over the historical period, mainly in the Southern Ocean and the equatorial Pacific. This raises concerns that the CMIP5 models may also underestimate future uptake of anthropogenic CO₂, which would lead to an overestimation of carbon–climate feedbacks. What are potential causes for the relatively small anthropogenic CO₂ uptake in the CMIP5 models? Deficiencies in the underlying climatological Southern Ocean circulation of the models may explain part of the discrepancies. A large fraction of the anthropogenic CO₂ uptake accumulates in the Subantarctic Mode Water and Antarctic Intermediate Water and flows into other ocean basins (Sabine et al. 2004). These water masses are generally poorly represented in the CMIP5 models (Sallée et al.

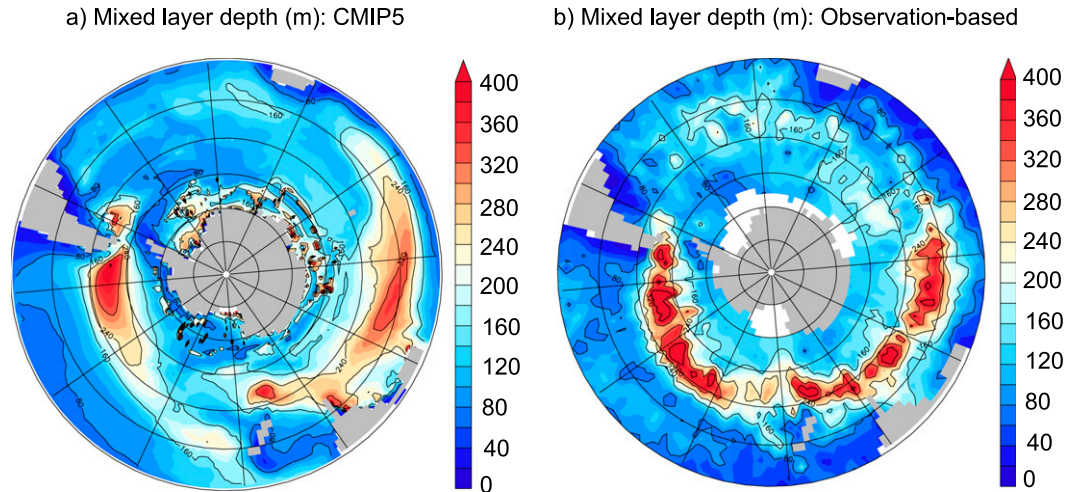


FIG. 10. (a) CMIP5 multimodel mean representation of September mixed-layer depths averaged over the first 20 years of the historical simulation. (b) Observation-based September mixed-layer depth climatology from de Boyer Montégut et al. (2004). The mixed-layer depths are diagnosed in a consistent fashion across all of the CMIP5 model and observations using a density criterion of 0.03 kg m^{-3} relative to the surface. This criterion has been found to be a reasonable measure of the mixed-layer depth in the Southern Ocean in recent studies (e.g., Sallée et al. 2013b). The following 13 CMIP5 models are used: CNRM-CM5, IPSL-CM5A-LR, IPSL-CM5A-MR, IPSL-CM5B-LR, HadEM2-CC, MPI-ESM-LR, MRI-CGCM3, GISS-E2-R, CCSM4, NorESM1-M, GFDL-CM3, GFDL-ESM2G, and GFDL-ESM2M.

2013b; Meijers 2014). The characteristics of mode and intermediate water appear to be tightly linked to the characteristics of simulated winter mixed-layer depths (Sallée et al. 2013b). Figure 10 shows that the CMIP5 models as a class underestimate the winter mixed-layer depth in the Southern Ocean, mainly in the Indian Ocean sector and the Pacific Ocean sector, where the winter mixed layers are also too far equatorward. This shallow bias and equatorward shift may cause too-large formation of subtropical mode waters rather than formation of Subantarctic Mode Waters, which is subsequently penetrated less deeply and at lighter water mass classes (Sallée et al. 2013b). Sallée et al. (2013a) showed that this shallow mixed-layer bias is likely associated with an excess freshwater input at the sea surface that overstratifies the surface layer and prevents deep ocean convection from developing in the winter. However, biases in the representation of the oceanic buffer capacity and biases in the observation-based estimates of anthropogenic carbon may also contribute to the model–data differences, although the former has not yet been investigated in depth in the CMIP5 models. The ΔC^* method may have a positive bias of about 7% in the global anthropogenic carbon estimate (Matsumoto and Gruber 2005), and the TTD method largely overestimates the deep Southern Ocean anthropogenic carbon storage (Vaugh et al. 2006). Gerber et al. (2009) show that using different anthropogenic carbon storage estimates for the inversion could result in

Southern Ocean anthropogenic CO_2 flux estimates that differ by a factor of 2. However, Gerber et al. (2009) also included anthropogenic carbon estimates from methods with well-known deficiencies, such as the Tracer combining Oxygen, inorganic Carbon and total Alkalinity (TrOCA) method (Yool et al. 2010), that were not used in this study. In addition, observation-based estimates assume a steady-state ocean. The effect of changes in ocean circulation on anthropogenic carbon uptake over the historical period as simulated by the CMIP5 models, however, is $\pm 5 \text{ Pg C}$ and thus much smaller than the difference between the models and the observation-based estimates.

Interestingly, the simulated changes in global ocean heat content are in good agreement with observation-based estimates over the period 1960–2005 despite the fact that the simulated anthropogenic CO_2 uptake is underestimated. This may again point toward different mechanisms controlling ocean carbon and heat uptake. However, uncertainties in the simulated radiative forcing strength, particularly from non- CO_2 radiative forcing agents, may also play a role here.

Recent analysis indicates a stalling of the Southern Ocean CO_2 sink despite an increase in atmospheric CO_2 over recent decades [Le Quéré et al. (2007); note that other atmospheric inversion studies questioned the evidence for a reduced efficiency (e.g., Law et al. 2008)]. Follow-up studies attribute the stalling to an enhanced outgassing of natural carbon over recent decades driven by an acceleration of the Southern Ocean overturning

linked to poleward intensified westerlies (e.g., Lovenduski et al. 2008). By analyzing chlorofluorocarbons, Waugh et al. (2013) show that mode waters are indeed getting younger and Circumpolar Deep Waters are getting older, consistent with the idea of an intensifying Southern Ocean overturning. In light of these results, one might also expect an outgassing of natural CO₂ in the CMIP5 models with climate change, since almost all CMIP5 models simulate a poleward shift and intensification of the Southern Hemisphere westerlies over the historical period (Bracegirdle et al. 2013). However, the CMIP5 models as a class simulate a very small effect of climate change on the net carbon uptake over the historical period on the order of ± 5 Pg C. This is consistent with offline global ocean biogeochemical models forced by atmospheric fields from reanalysis products, which simulate changes in the natural carbon over the historical period of about ± 5 Pg C (Le Quéré et al. 2010; Majkut et al. 2014a). In any case, the weakening of the net Southern Ocean CO₂ sink as suggested by recent studies is small and may be difficult to reproduce in the CMIP5 models given the relatively large simulated decadal-scale variability in CO₂ uptake by the Southern Ocean.

Current CMIP5 models are unable to resolve meso-scale eddies that may play a major role in how the Southern Ocean responds to changes in climate forcing. A number of studies using eddy-permitting ocean models show that the Southern Ocean meridional overturning circulation may be less sensitive to changes in wind stress than simulated with coarse-resolution models because of a stronger southward eddy-driven overturning compensation (e.g., Hallberg and Gnanadesikan 2006; Farneti et al. 2010; Meredith et al. 2012; Dufour et al. 2012; Morrison and Hogg 2013). Morrison and Hogg (2013) use eddy-resolving ocean model configurations ($1/16^\circ$ resolution) to show that a doubling of wind stress results in a 70% increase of the overturning, less than simulated with coarse-resolution models. A reduced sensitivity of the overturning may therefore result in an overall reduced sensitivity of the natural carbon cycle to changes in wind stress, as has been recently shown in an eddy-permitting model (Munday et al. 2014). In other words, coarse-resolution CMIP5 models may overestimate the natural carbon cycle response to past and future changes in wind stress. Next-generation high-resolution Earth system models will hopefully improve our understanding of the role of eddies for carbon and heat uptake by the Southern Ocean.

We show that currently about 6% of the anthropogenic carbon and about 19% of the excess heat is stored below 2000-m depths, with the largest part (2% of global total anthropogenic carbon and 6% of global total

excess heat) located in the deep Southern Ocean south of 30°S. The CMIP5 results are qualitatively in line with observation studies, which suggest that the deep ocean, often omitted in heat and sea level rise budgets due to inadequacy of data records, plays an important role for the Earth's energy budget and for our understanding of past and current climate change (Purkey and Johnson 2012). However, year-round ocean temperature data are currently obtained from profiling floats, which are restricted to the upper 2000 m of the ocean and are thus not able to sample the entire ocean depth. As a result, there are not sufficient data to close the energy budget of the Earth (Trenberth and Fasullo 2010b) and to establish an observation-based relationship between the causes of the recent hiatus in global mean surface temperature (only a small global mean atmospheric surface temperature trend over the period 1998–2012) and deep ocean heat uptake (e.g., Meehl et al. 2011). Model data are often used to close this gap. This leads to the interesting question of whether the deep ocean heat storage as simulated by the CMIP5 models would be sufficient to explain the recent hiatus. Over the last 15 years of the historical simulation (1991–2005), the CMIP5 models store $8.3 \pm 3.8 \times 10^{22}$ J in the top 700 m, consistent with observation-based estimates (Fig. 7), $6.0 \pm 4.1 \times 10^{22}$ J below 700 m, and $2.8 \pm 3.2 \times 10^{22}$ J below 2000 m. We estimate that the anomalous cooling of about 0.1°C in ΔT over the recent 15-yr hiatus period resulted in an approximately anomalous energy imbalance ΔF of 2.7×10^{22} J ($\Delta F = \lambda \Delta T$) when using the mean climate feedback factor λ of $1.1 \text{ W m}^{-2} \text{ }^\circ\text{C}^{-1}$ from the CMIP5 models (Forster et al. 2013). If we assume that this extra energy of 2.7×10^{22} J got stored in the deep ocean below 700 m or even below 2000 m (e.g., Meehl et al. 2011), this would imply that the CMIP5 models would have to store an additional 45% of heat below 700 m or an additional 96% of heat below 2000 m. Therefore, for the hiatus to be solely explainable by deep ocean storage would require a substantial perturbation to ocean heat uptake below 700 m.

The data scarcity also applies to ocean biogeochemical properties. Estimates of changes in deep ocean biogeochemical properties rely mainly on data from a sparse set of recent ship observations or on model data, and thus long-term changes in biogeochemistry in the deep Southern Ocean are currently unknown. The fact that the CMIP5 multimodel spread in deep ocean anthropogenic CO₂ storage of ± 3 Pg C and excess heat storage of $\pm 5 \times 10^{22}$ J is similar in magnitude as the multimodel mean of 5 Pg C and 5×10^{22} J, respectively, highlights the need for new deep ocean measurement data to better constrain the model and ultimately the Earth energy (and carbon) budget.

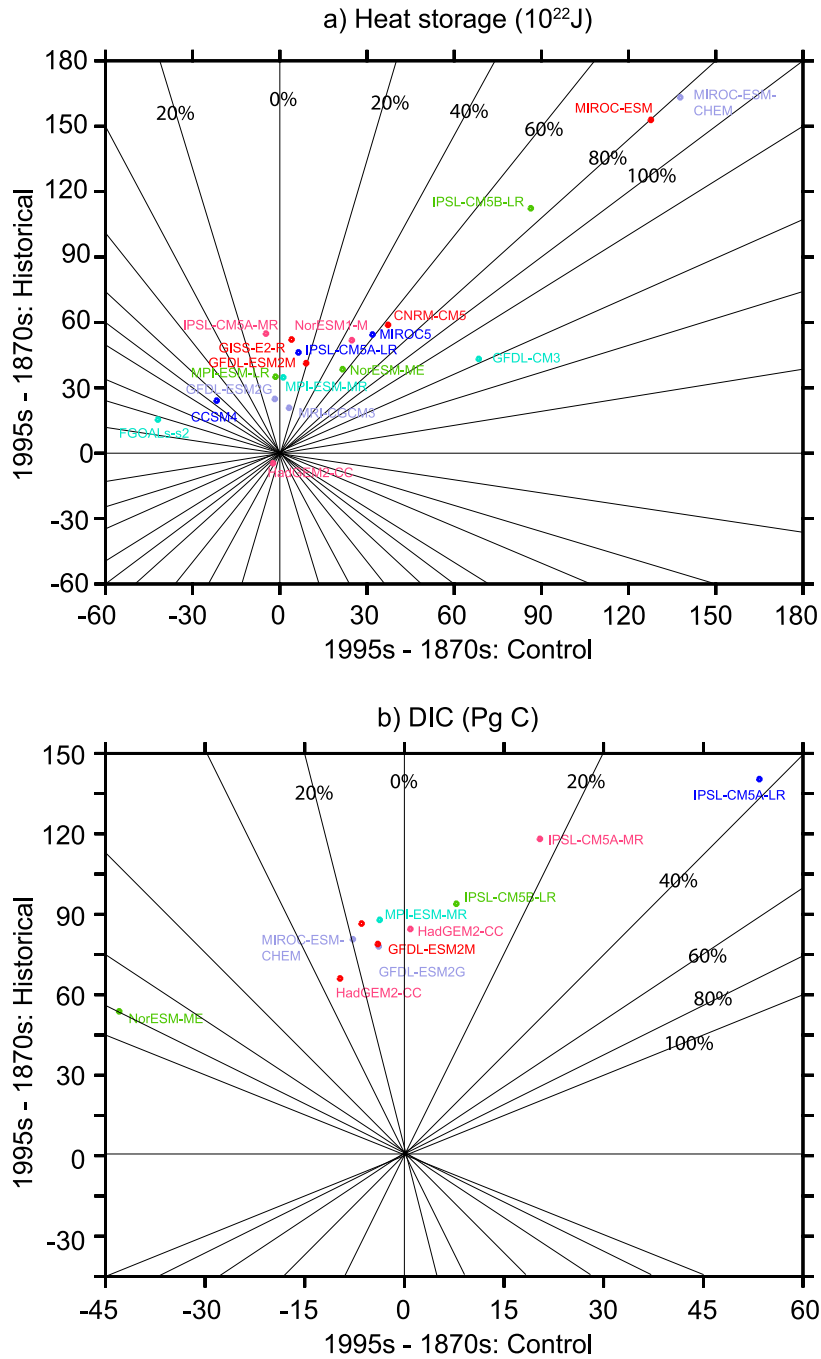


FIG. A1. Differences in global ocean (a) heat storage and (b) integrated DIC over the period 1870 (represented by mean of period 1861–80) to 1995 (represented by mean of period 1986–2005) in the historical CMIP5 simulations (not detrended) vs differences over the same period in the corresponding preindustrial control simulations. Global integrated DIC is given for the GLODAP dataset area only. Radiating lines indicate percentage values of the ratios between the simulated changes in the control simulations and the changes in the corresponding historical simulations.

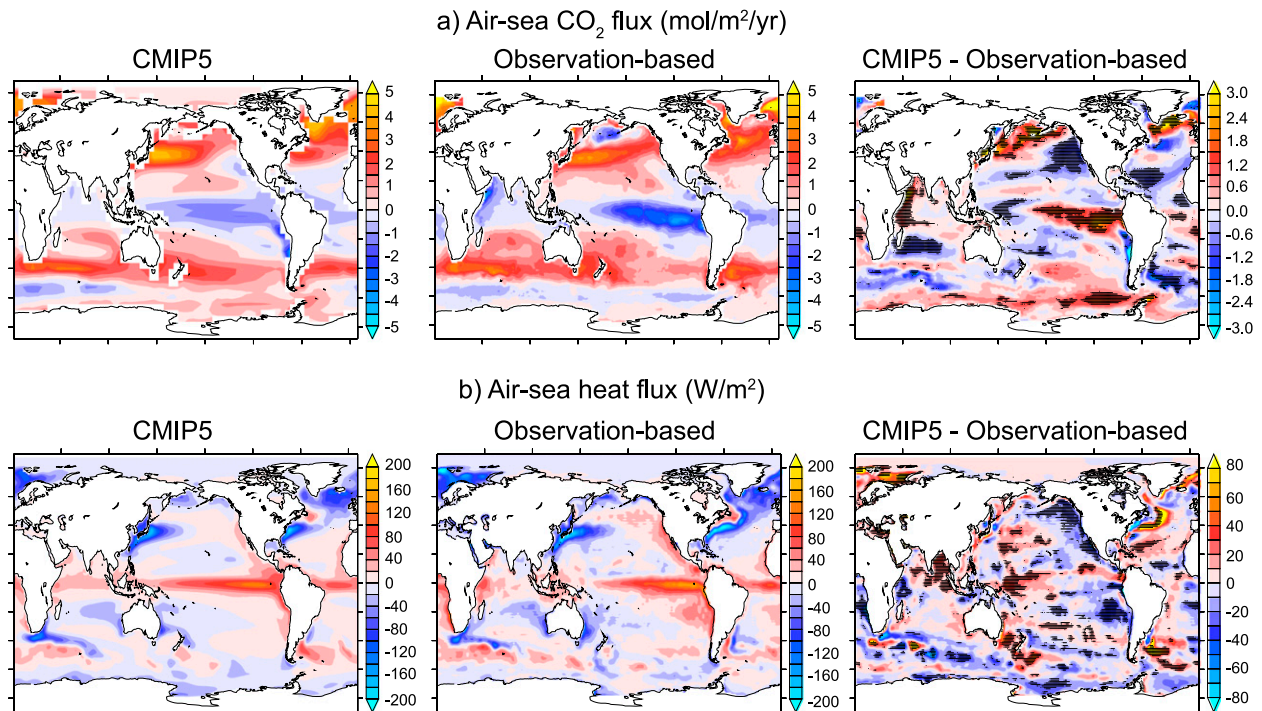


FIG. B1. Comparison of simulated multimodel mean (a) net air-sea CO_2 fluxes and net heat fluxes with observation-based estimates. Observation-based products are from Landschützer et al. (2014) for air-sea CO_2 fluxes and from the Coordinated Ocean-ice Reference Experiments, version 2 (CORE-2) dataset (Large and Yeager 2009) for net heat fluxes. Simulated air-sea CO_2 fluxes are averaged over the period 1996–2005 and observation-based air-sea CO_2 fluxes are averaged over the period 1998–2011. Simulated and observation-based net heat fluxes are averaged over the period 1986–2005. Stippled regions in the differences plots between model and observations correspond to regions in which at least 82% (air-sea CO_2 flux) and 84% (heat flux) of the models share a common positive or negative bias.

We conclude that the Southern Ocean south of 30°S accounts for $75\% \pm 22\%$ of the global excess heat uptake and $43\% \pm 3\%$ of the global anthropogenic CO_2 uptake over the period 1861–2005. The large intermodel variability in the Southern Ocean in the CMIP5 models, although reduced compared to earlier-generation climate models, also indicates that the exact processes governing the magnitude and regional distribution of heat and carbon uptake remain poorly understood. Better understanding of Southern Ocean processes are urgently needed to pin down one of the greatest sources of uncertainties in predictions of the fate of anthropogenic carbon and of the climate.

Acknowledgments. We thank N. Gruber, K. Rodgers, S. Mikaloff Fletcher, and S. Griffies for discussions, and K. Olivo, M. Harrison, and U. Beyerle, who helped postprocessing the CMIP5 data. We acknowledge the World Climate Research Programme’s Working Group on Coupled Modelling, which is responsible for CMIP, and we thank the climate modeling groups (listed in Table 1 of this paper) for producing and making available their model output. TLF acknowledges support by

the SNSF (Ambizione Grant PZ00PZ-14573) and the Carbon Mitigation Initiative with support from BP.

APPENDIX A

Model Drifts

In this appendix, we provide more details about drift in the CMIP5 models. In this study, we account for drifts in the preindustrial control simulations by calculating the climate deltas of the control simulation (e.g., $\Delta_{\text{control}} = \Delta_{\text{control},1995\text{s}} - \Delta_{\text{control},1870\text{s}}$) and the historical simulation (e.g., $\Delta_{\text{historical}} = \Delta_{\text{historical},1995\text{s}} - \Delta_{\text{historical},1870\text{s}}$), and then the total delta as the differences between the historical deltas and the control deltas ($\Delta = \Delta_{\text{historical}} - \Delta_{\text{control}}$). Most models exhibit global ocean heat storage drifts smaller than the magnitude of forced climate change (Fig. A1a). However, drifts in the preindustrial heat storage in GFDL CM3, MIROC-ESM-CHEM, and MIROC-ESM are equally as large as their respective transient ocean heat storage anomalies. Overall, the control drift in global integrated DIC is smaller than the drift in the ocean heat storage and accounts in all but

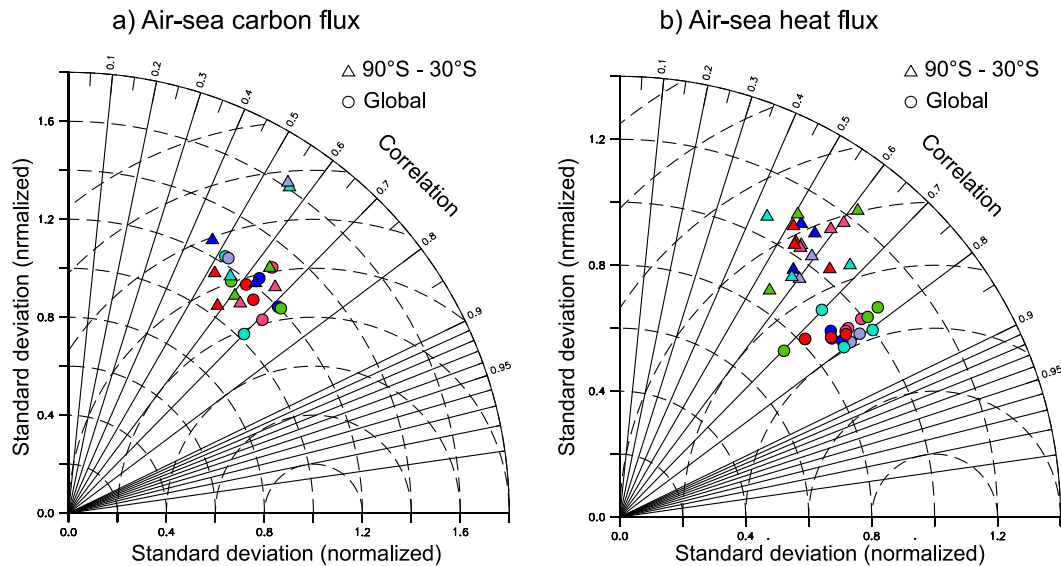


FIG. B2. Taylor diagrams showing information about the pattern similarity between simulated and observation-based results for (a) air–sea CO_2 fluxes and (b) net air–sea heat fluxes. Observation-based products are from Landschützer et al. (2014) for air–sea CO_2 fluxes and from the CORE-2 dataset (Large and Yeager 2009) for net heat fluxes. The angular coordinate indicates the correlation coefficient and the radial coordinate shows the normalized standard deviation ($\text{std}_{\text{model}}/\text{std}_{\text{obs}}$). The point at unit distance from the origin along the abscissa represents the observed field. Circles represent the global ocean, and triangles represent the Southern Ocean (90°–30°S).

the IPSL-CM5A-LR for less than 20% of the DIC changes over the historical period (Fig. A1b). In general, drift errors become increasingly important at regional scale. The drift in the models is largest in the abyssal ocean, whereas the signal of the historical simulation is mostly concentrated in the top few hundred meters. This is consistent with the results of Sen Gupta et al. (2013), who pointed out that the drift in ocean heat and carbon storage may dominate any forced change in the deep ocean. Reasons for drifts are manifold. Incomplete spinup of the climate models can cause drifts in preindustrial control simulations. Unphysical sources and sinks within climate models may also lead to spurious drifts.

APPENDIX B

Model Evaluations

Here, we briefly discuss the skill of the different CMIP5 models in representing spatial and temporal variability of present-day air–sea CO_2 fluxes and net air–sea heat fluxes (Figs. B1, B2). Further details about individual model performances are shown elsewhere (see individual references in Table 2).

The large-scale patterns of air–sea CO_2 fluxes are well represented in the CMIP5 models, with uptake simulated in the northern mid and high latitudes and the southern midlatitudes and release simulated in the

tropics and parts of the Southern Ocean (Fig. B1a). The primary CMIP5 multimodel mean bias patterns (stippling in Fig. B1a) include the smaller outgassing close to the Antarctic Continent and smaller outgassing in the eastern equatorial Pacific. The CMIP5 models as a class show similar biases in the Southern Ocean (triangles in Fig. B2a) and the global ocean (circles in Fig. B2a), with correlation coefficients ranging from 0.4 to 0.7. Note that in the Southern Ocean, the CMIP5 models agree better with the Landschützer et al. (2014) air–sea CO_2 fluxes than with the Takahashi et al. (2009) climatology (not shown). The Landschützer et al. (2014) product covers the period 1998–2011 and thus includes much more data from the Southern Ocean than the Takahashi et al. (2009) climatology. The observation-based CO_2 outgassing in the eastern equatorial Pacific may be particularly strong because of predominately La Niña conditions since the beginning of the twenty-first century, as the eastern equatorial CO_2 outgassing tends to be stronger during La Niña conditions. The CMIP5 models simulate their own natural variability and may thus be partly out of phase with the observed climate variability.

The CMIP5 models reasonably represent the net heat flux pattern (Fig. B1b). Correlations coefficients are about 0.6–0.7 for the global ocean and 0.4–0.7 for the Southern Ocean (Fig. B2b). The patchy stippling in Fig. B1 indicates that no systematic large-scale deviations are modeled. Note, however, that reanalysis

products share similar biases as the models, especially over the Southern Ocean (Trenberth and Fasullo 2010a). This makes a clean comparison of model data with reanalysis products difficult.

REFERENCES

- Arora, V. K., and Coauthors, 2013: Carbon-concentration and carbon-climate feedbacks in CMIP5 Earth system models. *J. Climate*, **26**, 5289–5314, doi:10.1175/JCLI-D-12-00494.1.
- Banks, H. T., and J. M. Gregory, 2006: Mechanisms of ocean heat uptake in a coupled climate model and the implications for tracer based predictions of ocean heat uptake. *Geophys. Res. Lett.*, **33**, L07608, doi:10.1029/2005GL025352.
- Bao, Q., and Coauthors, 2013: The flexible global ocean-atmosphere-land system model, Spectral Version 2: FGOALS-s2. *Adv. Atmos. Sci.*, **30**, 561–576, doi:10.1007/s00376-012-2113-9.
- Bentsen, M., and Coauthors, 2012: The Norwegian Earth System Model, NorESM1-M—Part 1: Description and basic evaluation. *Geosci. Model Dev. Discuss.*, **5**, 2843–2931, doi:10.5194/gmdd-5-2843-2012.
- Böning, C. W., A. Dispert, M. Visbeck, S. R. Rintoul, and F. U. Schwarzkopf, 2008: The response of the Antarctic Circumpolar Current to recent climate change. *Nat. Geosci.*, **1**, 864–869, doi:10.1038/ngeo362.
- Bracegirdle, T. J., E. Shuckburgh, J.-B. Sallee, Z. Wang, A. J. S. Meijers, N. Bruneau, T. Phillips, and L. J. Wilcox, 2013: Assessment of surface winds over the Atlantic, Indian, and Pacific Ocean sectors of the Southern Ocean in CMIP5 models: Historical bias, forcing response, and state dependence. *J. Geophys. Res. Atmos.*, **118**, 547–562, doi:10.1002/jgrd.50153.
- Bryan, K., 1969: Climate and the ocean circulation III. The ocean model. *Mon. Wea. Rev.*, **97**, 806–827, doi:10.1175/1520-0493(1969)097<0806:CATOC>2.3.CO;2.
- Caldeira, K., and P. B. Duffy, 2000: The role of the Southern Ocean in uptake and storage of anthropogenic carbon dioxide. *Science*, **287**, 620–622, doi:10.1126/science.287.5453.620.
- Cheng, W., J. C. H. Chiang, and D. Zhang, 2013: Atlantic meridional overturning circulation (AMOC) in CMIP5 models: RCP and historical simulations. *J. Climate*, **26**, 7187–7197, doi:10.1175/JCLI-D-12-00496.1.
- Church, J. A., J. S. Godfrey, D. R. Jackett, and T. J. McDougall, 1991: A model of sea level rise caused by ocean thermal expansion. *J. Climate*, **4**, 438–456, doi:10.1175/1520-0442(1991)004<0438:AMOSLR>2.0.CO;2.
- de Boyer Montégut, C., G. Madec, A. S. Fischer, A. Lazar, and D. Iudicone, 2004: Mixed layer depth over the global ocean: An examination of profile data and a profile-based climatology. *J. Geophys. Res.*, **109**, C12003, doi:10.1029/2004JC002378.
- Domingues, C. M., J. A. Church, N. J. White, P. J. Gleckler, S. E. Wijffels, P. M. Barker, and J. R. Dunn, 2008: Improved estimates of upper-ocean warming and multi-decadal sea-level rise. *Nature*, **453**, 1090–1093, doi:10.1038/nature07080.
- Doney, S. C., and Coauthors, 2004: Evaluating global ocean carbon models: The importance of realistic physics. *Global Biogeochem. Cycles*, **18**, GB3017, doi:10.1029/2003GB002150.
- Downes, S. M., N. L. Bindoff, and S. R. Rintoul, 2010: Changes in the subduction of Southern Ocean water masses at the end of the twenty-first century in eight IPCC models. *J. Climate*, **23**, 6526–6541, doi:10.1175/2010JCLI3620.1.
- Dufour, C. O., J. Le Sommer, J. D. Zika, M. Gehlen, J. C. Orr, P. Mathiot, and B. Barnier, 2012: Standing and transient eddies in the response of the Southern Ocean meridional overturning to the southern annular mode. *J. Climate*, **25**, 6958–6974, doi:10.1175/JCLI-D-11-00309.1.
- Dufresne, J.-L., and Coauthors, 2013: Climate change projections using the IPSL-CM5 Earth System Model: From CMIP3 to CMIP5. *Climate Dyn.*, **40**, 2123–2165, doi:10.1007/s00382-012-1636-1.
- Dunne, J. P., and Coauthors, 2012: GFDL's ESM2 global coupled climate-carbon Earth System Models part I: Physical formulation and baseline simulation characteristics. *J. Climate*, **25**, 6646–6665, doi:10.1175/JCLI-D-11-00560.1.
- , and Coauthors, 2013: GFDL's ESM2 global coupled climate-carbon Earth System Models. Part II: Carbon system formulation and baseline simulation characteristics. *J. Climate*, **26**, 2247–2267, doi:10.1175/JCLI-D-12-00150.1.
- Farneti, R., T. L. Delworth, A. J. Rosati, S. M. Griffies, and F. R. Zeng, 2010: The Role of mesoscale eddies in the rectification of the Southern Ocean response to climate change. *J. Phys. Oceanogr.*, **40**, 1539–1557, doi:10.1175/2010JPO4353.1.
- Forster, P. M., T. Andrews, P. Good, J. M. Gregory, L. S. Jackson, and M. Zelinka, 2013: Evaluating adjusted forcing and model spread for historical and future scenarios in the CMIP5 generation of climate models. *J. Geophys. Res.*, **118**, 1139–1150, doi:10.1002/jgrd.50174.
- Friedlingstein, P., and Coauthors, 2006: Climate-carbon cycle feedback analysis: Results from the C⁴MIP model intercomparison. *J. Climate*, **19**, 3337–3353, doi:10.1175/JCLI3800.1.
- Frölicher, T. L., F. Joos, and C. C. Raible, 2011: Sensitivity of atmospheric CO₂ and climate to explosive volcanic eruptions. *Biogeosciences*, **8**, 2317–2339, doi:10.5194/bg-8-2317-2011.
- , M. Winton, and J. L. Sarmiento, 2014: Continued global warming after CO₂ emissions stoppage. *Nat. Climate Change*, **4**, 40–44, doi:10.1038/nclimate2060.
- Gent, P. R., and Coauthors, 2011: The Community Climate System Model version 4. *J. Climate*, **24**, 4973–4991, doi:10.1175/2011JCLI4083.1.
- Gerber, M., F. Joos, M. Vázquez-Rodríguez, F. Touratier, and C. Goyet, 2009: Regional air-sea fluxes of anthropogenic carbon inferred with an Ensemble Kalman Filter. *Global Biogeochem. Cycles*, **23**, GB1013, doi:10.1029/2008GB003247.
- Gille, S., 2002: Warming of the Southern Ocean since the 1950s. *Science*, **295**, 1275–1277, doi:10.1126/science.1065863.
- Giorgetta, M. A., and Coauthors, 2013: Climate and carbon cycle changes from 1850 to 2100 in MPI-ESM simulations for the Coupled Model Intercomparison Project phase 5. *J. Adv. Model. Earth Syst.*, **5**, 572–597, doi:10.1002/jame.20038.
- Gregory, J. M., and Coauthors, 2013: Climate models without preindustrial volcanic forcing underestimate historical ocean thermal expansion. *Geophys. Res. Lett.*, **40**, 1600–1604, doi:10.1002/grl.50339.
- Griffies, S. M., and Coauthors, 2011: The GFDL CM3 Coupled Climate Model: Characteristics of the ocean and sea ice simulations. *J. Climate*, **24**, 3520–3544, doi:10.1175/2011JCLI3964.1.
- Gruber, N., J. L. Sarmiento, and T. F. Stocker, 1996: An improved method for detecting anthropogenic CO₂ in the oceans. *Global Biogeochem. Cycles*, **10**, 809–837, doi:10.1029/96GB01608.
- Hallberg, R., and A. Gnanadesikan, 2006: The role of eddies in determining the structure and response of the wind-driven Southern Hemisphere overturning: Results from the Modeling Eddies in the Southern Ocean (MESO) project. *J. Phys. Oceanogr.*, **36**, 2232–2252, doi:10.1175/JPO2980.1.

- Ishii, M., and M. Kimoto, 2009: Reevaluation of historical ocean heat content variations with time-varying XBT and MBT depth bias corrections. *J. Oceanogr.*, **65**, 287–299, doi:10.1007/s10872-009-0027-7.
- Khaliwala, S., F. Primeau, and T. Hall, 2009: Reconstruction of the history of anthropogenic CO₂ concentrations in the ocean. *Nature*, **462**, 346–349, doi:10.1038/nature08526.
- Knutti, R., D. Masson, and A. Gettelman, 2013: Climate model genealogy: Generation CMIP5 and how we got there. *Geophys. Res. Lett.*, **40**, 1194–1199, doi:10.1002/grl.50256.
- Landschützer, P., N. Gruber, D. C. E. Bakker, and U. Schuster, 2014: Recent variability of the global ocean carbon sink. *Global Biogeochem. Cycles*, **28**, 927–949, doi:10.1002/2014GB004853.
- Large, W. G., and S. G. Yeager, 2009: The global climatology of an interannually varying air–sea flux data set. *Climate Dyn.*, **33**, 341–364, doi:10.1007/s00382-008-0441-3.
- Law, R. M., R. J. Matear, and R. J. Francey, 2008: Comment on “Saturation of the Southern Ocean CO₂ sink due to recent climate change.” *Science*, **319**, 5863, doi:10.1126/science.1149077.
- Le Quéré, C., and Coauthors, 2007: Saturation of the Southern Ocean CO₂ sink due to recent climate change. *Science*, **316**, 1735–1738, doi:10.1126/science.1136188.
- , T. Takahashi, E. T. Buitenhuis, C. Rödenbeck, and S. C. Sutherland, 2010: Impact of climate change and variability on the global oceanic sink of CO₂. *Global Biogeochem. Cycles*, **24**, GB4007, doi:10.1029/2009GB003599.
- Lenton, A., R. J. Matear, and B. Tilbrook, 2006: Design of an observational strategy for quantifying the Southern Ocean uptake of CO₂. *Global Biogeochem. Cycles*, **20**, GB4010, doi:10.1029/2005GB002620.
- , F. Codron, L. Bopp, N. Metzl, P. Cadule, A. Tagliabue, and J. Le Sommer, 2009: Stratospheric ozone depletion reduces ocean carbon uptake and enhances ocean acidification. *Geophys. Res. Lett.*, **36**, L12606, doi:10.1029/2009GL038227.
- Levitus, S., J. I. Antonov, T. P. Boyer, R. A. Locarnini, H. E. Garcia, and A. V. Mishonov, 2009: Global ocean heat content 1955–2008 in light of recently revealed instrumentation problems. *Geophys. Res. Lett.*, **36**, L07608, doi:10.1029/2008GL037155.
- Lo Monaco, C., C. Goyet, N. Metzl, A. Poisson, and F. Touratier, 2005: Distribution and inventory of anthropogenic CO₂ in the Southern Ocean: Comparison of three data-based methods. *J. Geophys. Res.*, **110**, C09S02, doi:10.1029/2004JC002571.
- Lovenduski, N. S., N. Gruber, and S. C. Doney, 2008: Toward a mechanistic understanding of the decadal trends in the Southern Ocean carbon sink. *Global Biogeochem. Cycles*, **22**, GB3016, doi:10.1029/2007GB003139.
- Lyman, J. M., S. A. Good, V. V. Gouretski, M. Ishii, G. C. Johnson, M. D. Palmer, D. M. Smith, and J. K. Willis, 2010: Robust warming of the global upper ocean. *Nature*, **465**, 334–337, doi:10.1038/nature09043.
- Majkut, J. D., B. R. Carter, T. L. Frölicher, C. O. Dufour, K. B. Rodgers, and J. L. Sarmiento, 2014a: An observing system simulation for Southern Ocean carbon dioxide uptake. *Philos. Trans. Roy. Soc. London*, **A372**, 20130046, doi:10.1098/rsta.2013.0046.
- , J. L. Sarmiento, and K. B. Rodgers, 2014b: A growing oceanic carbon uptake: Results from an inversion study of surface pCO₂ data. *Global Biogeochem. Cycles*, **28**, 335–351, doi:10.1002/2013GB004585.
- Manabe, S., R. J. Stouffer, M. J. Spelman, and K. Bryan, 1991: Transient responses of a coupled ocean–atmosphere model to gradual changes of atmospheric CO₂. Part I: Annual mean response. *J. Climate*, **4**, 785–818, doi:10.1175/1520-0442(1991)004<0785:TROACO>2.0.CO;2.
- Manning, A. C., and R. F. Keeling, 2006: Global oceanic and land biotic sinks from the Scripps atmospheric oxygen flask sampling network. *Tellus*, **58B**, 95–116, doi:10.1111/j.1600-0889.2006.00175.x.
- Marshall, J., and K. Speer, 2012: Closure of the meridional overturning circulation through Southern Ocean upwelling. *Nat. Geosci.*, **5**, 171–180, doi:10.1038/ngeo1391.
- Martin, G. M., and Coauthors, 2011: The HadGEM2 family of Met Office Unified Model climate configurations. *Geosci. Model Dev.*, **4**, 723–757, doi:10.5194/gmd-4-723-2011.
- Matsumoto, K., and N. Gruber, 2005: How accurate is the estimation of anthropogenic carbon in the ocean? An evaluation of the ΔC* method. *Global Biogeochem. Cycles*, **19**, GB3014, doi:10.1029/2004GB002397.
- Matthews, H. D., N. Gillet, P. Stott, and K. Zickfeld, 2009: The proportionality of global warming to cumulative carbon emissions. *Nature*, **459**, 829–832, doi:10.1038/nature08047.
- Meehl, G. A., J. M. Arblaster, J. T. Fasullo, A. Hu, and K. E. Trenberth, 2011: Model-based evidence of deep-ocean heat uptake during surface-temperature hiatus periods. *Nat. Climate Change*, **1**, 360–364, doi:10.1038/nclimate1229.
- Meijers, A. J. S., 2014: The Southern Ocean in the Coupled Model Intercomparison Project phase 5. *Philos. Trans. Roy. Soc. London*, **A372**, 20130296, doi:10.1098/rsta.2013.0296.
- Meredith, M. P., A. C. Naveira Garabato, A. M. Hogg, and R. Farneti, 2012: Sensitivity of the overturning circulation in the Southern Ocean to decadal changes in wind forcing. *J. Climate*, **25**, 99–110, doi:10.1175/2011JCLI4204.1.
- Mikaloff Fletcher, S. E., and Coauthors, 2006: Inverse estimates of anthropogenic CO₂ uptake, transport, and storage by the ocean. *Global Biogeochem. Cycles*, **20**, GB2002, doi:10.1029/2005GB002530.
- Morrison, A. K., and A. M. Hogg, 2013: On the relationship between Southern Ocean overturning and ACC transport. *J. Phys. Oceanogr.*, **43**, 140–148, doi:10.1175/JPO-D-12-057.1.
- Munday, D. R., H. L. Johnson, and D. P. Marshall, 2014: Impact and effects of mesoscale ocean eddies on ocean carbon storage and atmospheric pCO₂. *Global Biogeochem. Cycles*, **28**, 877–896, doi:10.1002/2014GB004836.
- Orr, J. C., and Coauthors, 2001: Estimates of anthropogenic carbon uptake from four three-dimensional global ocean models. *Global Biogeochem. Cycles*, **15**, 43–60, doi:10.1029/2000GB001273.
- Palmer, M. D., K. Haines, S. F. B. Tett, and T. J. Ansell, 2007: Isolating the signal of ocean global warming. *Geophys. Res. Lett.*, **34**, L23610, doi:10.1029/2007GL031712.
- Pardo, P. C., F. F. Pérez, S. Khaliwala, and A. F. Rios, 2014: Anthropogenic CO₂ estimates in the Southern Ocean: Storage partitioning in the different water masses. *Prog. Oceanogr.*, **120**, 230–242, doi:10.1016/j.pocean.2013.09.005.
- Pendergrass, A. G., and D. L. Hartmann, 2014: The atmospheric energy constraint on global-mean precipitation change. *J. Climate*, **27**, 757–768, doi:10.1175/JCLI-D-13-00163.1.
- Purkey, S. G., and G. C. Johnson, 2012: Global contraction of Antarctic Bottom Water between the 1980s and 2000s. *J. Climate*, **25**, 5830–5844, doi:10.1175/JCLI-D-11-00612.1.
- Regnier, P., and Coauthors, 2013: Anthropogenic perturbation of the carbon fluxes from land to ocean. *Nat. Geosci.*, **6**, 597–607, doi:10.1038/ngeo1830.

- Rignot, E., and Coauthors, 2008: Recent Antarctic ice mass loss from radar interferometry and regional climate modelling. *Nat. Geosci.*, **1**, 106–110, doi:10.1038/ngeo102.
- Roy, T., and Coauthors, 2011: Regional impacts of climate change and atmospheric CO₂ on future ocean carbon uptake: A multimodel linear feedback analysis. *J. Climate*, **24**, 2300–2318, doi:10.1175/2010JCLI3787.1.
- Russell, J. L., R. J. Stouffer, and K. W. Dixon, 2006: Intercomparison of the Southern Ocean circulations in IPCC coupled model control simulations. *J. Climate*, **19**, 4560–4575, doi:10.1175/JCLI3869.1.
- Sabine, C. L., and Coauthors, 2004: The ocean sink for anthropogenic CO₂. *Science*, **305**, 367–371, doi:10.1126/science.1097403.
- Sallée, J.-B., E. Shuckburgh, N. Bruneau, A. J. S. Meijers, T. J. Bracegirdle, and Z. Wang, 2013a: Assessment of Southern Ocean mixed-layer depths in CMIP5 models: Historical bias and forcing response. *J. Geophys. Res. Oceans*, **118**, 1845–1862, doi:10.1002/jgrc.20157.
- , —, —, —, —, —, and T. Roy, 2013b: Assessment of the Southern Ocean water mass circulation and characteristics in CMIP5 models: Historical bias and forcing response. *J. Geophys. Res.*, **118**, 1830–1844, doi:10.1002/jgrc.20135.
- Sarmiento, J. L., T. M. C. Hughes, R. J. Stouffer, and S. Manabe, 1998: Simulated response of the ocean carbon cycle to anthropogenic climate warming. *Nature*, **393**, 245–249, doi:10.1038/30455.
- , N. Gruber, M. A. Brzezinski, and J. P. Dunne, 2004: High-latitude controls of thermocline nutrients and low latitude biological productivity. *Nature*, **427**, 56–60, doi:10.1038/nature02127.
- Sen Gupta, A., A. Santoso, A. S. Taschetto, C. C. Ummerhofer, J. Trevena, and M. H. England, 2009: Projected changes to the Southern Hemisphere Ocean and Sea ice in the IPCC AR4 climate models. *J. Climate*, **22**, 3047–3078, doi:10.1175/2008JCLI2827.1.
- , N. C. Jourdain, J. N. Brown, and D. Monselesan, 2013: Climate Drift in the CMIP5 models. *J. Climate*, **26**, 8597–8615, doi:10.1175/JCLI-D-12-00521.1.
- Shindell, D. T., and Coauthors, 2013: Interactive ozone and methane chemistry in GISS-E2 historical and future climate simulations. *Atmos. Chem. Phys.*, **13**, 2653–2689, doi:10.5194/acp-13-2653-2013.
- Steinacher, M., and Coauthors, 2010: Projected 21st century decrease in marine productivity: A multi-model analysis. *Biogeosciences*, **7**, 979–1005, doi:10.5194/bg-7-979-2010.
- Takahashi, T., and Coauthors, 2009: Climatological mean and decadal change in surface ocean pCO₂, and net sea–air CO₂ flux over the global oceans. *Deep-Sea Res. II*, **56**, 554–577, doi:10.1016/j.dsr2.2008.12.009.
- Taylor, K. E., R. J. Stouffer, and G. A. Meehl, 2012: An overview of CMIP5 and the experiment design. *Bull. Amer. Meteor. Soc.*, **93**, 485–498, doi:10.1175/BAMS-D-11-00094.1.
- Thompson, D. W. J., S. Solomon, P. J. Kushner, M. H. England, K. M. Grise, and D. J. Karoly, 2011: Signatures of the Antarctic ozone hole in Southern Hemisphere surface climate change. *Nat. Geosci.*, **4**, 741–749, doi:10.1038/ngeo1296.
- Toggweiler, J. R., and B. Samuels, 1995: Effect of drake passage on the global thermohaline circulation. *Deep-Sea Res. I*, **42**, 477–500, doi:10.1016/0967-0637(95)00012-U.
- Trenberth, K. E., and J. T. Fasullo, 2010a: Simulation of present-day and twenty-first-century energy budgets of the southern oceans. *J. Climate*, **23**, 440–454, doi:10.1175/2009JCLI3152.1.
- , and —, 2010b: Tracking Earth's energy. *Science*, **328**, 316–317, doi:10.1126/science.1187272.
- Vázquez-Rodríguez, M., and Coauthors, 2009: Anthropogenic carbon distributions in the Atlantic Ocean: Data-based estimates from the Arctic to the Antarctic. *Biogeosciences*, **6**, 439–451, doi:10.5194/bg-6-439-2009.
- Voldoire, A., and Coauthors, 2013: The CNRM-CM5.1 global climate model: Description and basic evaluation. *Climate Dyn.*, **40**, 2091–2121, doi:10.1007/s00382-011-1259-y.
- Wanninkhof, R., and Coauthors, 2013: Global ocean carbon uptake: Magnitude, variability and trends. *Biogeosciences*, **10**, 1983–2000, doi:10.5194/bg-10-1983-2013.
- Watanabe, M., and Coauthors, 2010: Improved climate simulation by MIROC5: Mean states, variability, and climate sensitivity. *J. Climate*, **23**, 6312–6335, doi:10.1175/2010JCLI3679.1.
- Watanabe, S., and Coauthors, 2011: MIROC-ESM 2010: Model description and basic results of CMIP5-20c3m experiments. *Geosci. Model Dev.*, **4**, 845–872, doi:10.5194/gmd-4-845-2011.
- Watson, A. J., and J. C. Orr, 2003: Carbon dioxide fluxes in the global ocean. *Ocean Biogeochemistry*, M. J. R. Fasham, Ed., Springer, 123–141.
- Waugh, D. W., T. M. Hall, B. I. McNeil, R. Key, and R. J. Matear, 2006: Anthropogenic CO₂ in the oceans estimated using transit time distributions. *Tellus*, **58B**, 376–389, doi:10.1111/j.1600-0889.2006.00222.x.
- , F. Primeau, T. DeVries, and M. Holzer, 2013: Recent changes in the ventilation of the southern oceans. *Science*, **339**, 568–570, doi:10.1126/science.1225411.
- Winton, M., S. M. Griffies, B. L. Samuels, J. L. Sarmiento, and T. L. Frölicher, 2013: Connecting changing ocean circulation with changing climate. *J. Climate*, **26**, 2268–2278, doi:10.1175/JCLI-D-12-00296.1.
- Xie, P., and G. K. Vallis, 2012: The passive and active nature of ocean heat uptake in idealized climate change experiments. *Climate Dyn.*, **38**, 667–684, doi:10.1007/s00382-011-1063-8.
- Yool, A., A. Oschlies, A. J. G. Nurser, and N. Gruber, 2010: A model-based assessment of the TrOCA approach for estimating anthropogenic carbon in the ocean. *Biogeosciences*, **7**, 723–751, doi:10.5194/bg-7-723-2010.
- Yukimoto, S., and Coauthors, 2012: A new global climate model of the Meteorological Research Institute: MRI-CGCM3—Model description and basic performance. *J. Meteor. Soc. Japan*, **90A**, 23–64, doi:10.2151/jmsj.2012-A02.
- Zhang, R. T., and Coauthors, 2013: Have aerosols caused the observed Atlantic multidecadal variability? *J. Atmos. Sci.*, **70**, 1135–1144, doi:10.1175/JAS-D-12-0331.1.